Dallas-Fort Worth Modeling Support: Improving Vertical Mixing, Plume-in-Grid, and Photolysis Rates in CAMx

Prepared for:
Texas Commission on Environmental Quality
121 Park 35 Circle MC 164
Austin, TX 78753

Prepared by:
ENVIRON International Corporation
773 San Marin Drive, Suite 2115
Novato, California, 94945
www.environcorp.com
P-415-899-0700
F-415-899-0707

August 2012
06-26408F

ENVIRON

CONTENTS

EXECUTIVE SUMMARY 1

1.0 INTRODUCTION 3

1.1 Purpose 3

2.0 WRFCAMX EFFICIENCY IMPROVEMENTS 4

2.1 Approach 4

2.2 Results 5

2.2.1 Reading Direct Access Files 5

2.2.2 Profiler Results 6

3.0 VERTICAL MIXING IMPROVEMENTS 8

3.1 Background 8

3.2 Approach 9

3.3 Modeling Results 10

3.3.1 Statistical Performance in DFW 23

4.0 MODIFICATIONS TO PIG NIGHTTIME GROWTH RATES 26

4.1 Background 26

4.2 Approach 27

4.3 Results 29

4.3.1 Impacts at Rural Monitoring Sites 32

4.3.2 Impacts on CAMx Runtime 32

5.0 ENVIRONMENTAL FACTORS AFFECTING PHOTOLYSIS REACTIONS 40

5.1 Technical Analyses 40

5.1.1 NO_2 Photolysis 41

5.1.2 O_3 Photolysis 41

5.1.3 HCHO Photolysis 42

5.1.4 CH_3CHO Photolysis 43

5.1.5 Using TUV to Calculate Photolysis Adjustment Factors 44

5.2 Results 45

6.0 CONCLUSION AND RECOMMENDATIONS 48

6.1 WRFCAMx Efficiency Improvements 48

6.2 Vertical Mixing Improvements 48
6.3 Modifications to PiG Nighttime Growth Rates 49
6.4 Photolysis Rate Adjustments 50

7.0 REFERENCES 51

Tables

Table 2-1. Comparison of execution times between the original and improved WRFCAMx program. Results for network I/O and local I/O cases are shown. 5

Table 3-1. Simulated PBL depths over Longview on June 2 and 7 according to unpatched Kv inputs. 20

Table 4-1. Horizontal size evolution of a single test puff under idealized stable conditions for four different growth rate configurations (see text for details). Puff widths are given in terms of "full width at half maximum" (FWHM). Values in black represent puffs below 4 km grid scale; value in blue would cause puff dumping to a 4 km grid; values in red would cause puff dumping to a 12 km grid. 28

Table 5-1. Factors used in CAMx for adjusting pre-computed photolysis rates for temperature and pressure deviations from standard conditions of 298 K and 1 atmosphere. 45

Figures

Figure 3-1. Kv profiles at 1300 CST, June 20, 2006 for a 4-km grid column over south-central Texas. The pre-adjusted Kv profile (blue) indicates shallow/weak mixing; the adjusted profile (red) accounts for mixing through the cloud depth. 11

Figure 3-2. PBL fields at 1300 CST, June 20, 2012 on the TCEQ Rider 8 4 km modeling grid derived from the un-patched (upper left) and patched (upper right) Kv fields. CAMx cloud field as optical depth (bottom) is shown for reference. 12

Figure 3-3. Ozone difference plots at noon, 6 PM, and 9 PM on June 20, 2006 over the 12 km CAMx modeling domain. Plots on the left show the differences caused by the introduction of the OB70 patch relative to the KV100 run; plots on the right show the differences caused by the introduction of the cloud patch relative to the OB70 run. 13

Figure 3-4. Hourly time series at Hinton of observed and CAMx simulated ozone (top) and NOx (bottom) during June 1-10, 2006. Blue dots are measurements, black line is the KV100 run, red dashed line is the OB70 run, and blue dashed line is the OB70+CLD run. 14

Figure 3-5. Hourly vertical Kv profiles at Hinton on the evening of June 15, 2006. Color assignments are the same as in Figure 3, but a "no patch" profile is added in green. Note x-axis scaling is different on the 5 PM plot.....15

Figure 3-6. Hourly time series at Houston East of observed and CAMx simulated ozone (top) and NOx (bottom) during June 1-10, 2006. Blue dots are measurements, black line is the KV100 run, red dashed line is the OB70 run, and blue dashed line is the OB70+CLD run.....17

Figure 3-7. Hourly time series at Pecan Valley of observed and CAMx simulated ozone (top) and NOx (bottom) during June 1-10, 2006. Blue dots are measurements, black line is the KV100 run, red dashed line is the OB70 run, and blue dashed line is the OB70+CLD run.....18

Figure 3-8. Hourly time series at Longview of observed and CAMx simulated ozone (top) and NOx (bottom) during June 1-10, 2006. Blue dots are measurements, black line is the KV100 run, red dashed line is the OB70 run, and blue dashed line is the OB70+CLD run.....19

Figure 3-9. Time series of Kv profiles over Longview on June 2 (left) and June 7 (right), before (top) and after (bottom) applying the cloud patch. 20

Figure 3-10. Time series of observed and simulated hourly ozone on June 2 at Longview. The blue dashed line shows the impact of the cloud patch. 21

Figure 3-11. Cloud optical depth (left) and ozone differences (right) caused by the cloud patch on June 7 at 10 AM, 12 PM, and 2 PM. 22

Figure 3-12. Daily model performance statistics for 1-hour ozone over 19 sites in DFW, June 1-15, 2006. 24

Figure 3-13. Daily model performance statistics for 1-hour ozone over 19 sites in DFW, June 16-30, 2006. 25

Figure 4-1. Simulated hourly ozone fields at 3 AM on June 26, 2006 for the Base run (top left), PiG Modification run (top right), and difference (bottom). 30

Figure 4-2. Simulated hourly ozone fields at 8 AM on June 13, 2006 for the Base run (top left), PiG Modification run (top right), and difference (bottom). 31

Figure 4-3. Rural ozone monitoring sites in eastern Texas evaluated for PiG plume impacts. 33

Figure 4-4. (Top) Time series of hourly observed and predicted ozone from the Base and PiG Modification runs at the Wamba monitoring site. (Bottom) Spatial distribution of hourly ozone differences between the Base and PiG Modification runs at the time of peak difference at the Wamba monitoring site.....34

Figure 4-5. (Top) Time series of hourly observed and predicted ozone from the Base and PiG Modification runs at the Clarksville monitoring site. (Bottom) Spatial distribution of hourly ozone differences between the Base and PiG Modification runs at the time of peak difference at the Clarksville monitoring site. 35

Figure 4-6. (Top) Time series of hourly observed and predicted ozone from the Base and PiG Modification runs at the Palestine monitoring site. (Bottom) Spatial distribution of hourly ozone differences between the Base and PiG Modification runs at the time of peak difference at the Palestine monitoring site. 36

Figure 4-7. Average diurnal distribution of the number of CAMx PiG puffs in the 36 km (top), 12 km (middle) and 4 km (bottom) modeling grids over the June 2006 modeling period. Results from Base and PiG Modification runs are shown. 38

Figure 4-8. Number of CAMx PiG puffs each hour in the 4 km modeling grid over the June 2006 modeling period. 39

Figure 5-1. Absorption cross-section (σ; 10-20 cm^{-2}) for NO_2 and quantum yield (ϕ) for production of O-atom at UV wavelengths from 280-420nm. 41

Figure 5-2. Absorption cross-section (σ; 10-20 cm^{-2}) for O_3 and quantum yield (ϕ) for production of $O(^1D)$-atom at UV wavelengths from 280-360nm. 42

Figure 5-3. Absorption cross-section (σ; 10-20 cm^{-2}) for HCHO. 43

Figure 5-4. Temperature and pressure dependencies of the quantum yields for HCHO photolysis to HCO + H (ϕ_1) or CO + H_2 (ϕ_2). (ϕ_2 is independent of temperature and pressure.) 43

Figure 5-5. Absorption cross-section (σ; 10-20 cm^{-2}) for CH_3CHO. 44

Figure 5-6. Pressure dependence of the quantum yield (ϕ) for CH_3CHO photolysis to CH_3 + HCO. 44

Figure 5-7. Maximum (top) and minimum (bottom) difference in simulated 1-hour surface ozone concentration (ppb) on the 4 km grid over the entire June 2006 modeling period resulting from the addition of temperature and pressure adjustments on photolysis rates for NO_2, O_3, HCHO, and CH_3CHO. 46

Figure 5-8. Maximum (top) and minimum (bottom) difference in simulated 1-hour surface ozone concentration (ppb) on the 36 km grid over the entire June 2006 modeling period resulting from the addition of temperature and pressure adjustments on photolysis rates for NO_2, O_3, HCHO, and CH_3CHO. 47

EXECUTIVE SUMMARY

The purpose of this project was to improve the quality of TCEQ's photochemical modeling for Texas using CAMx by improving the treatment of vertical mixing, refining nocturnal plume growth rates within the Plume-in-Grid (PiG) sub-model, and accounting for environmental factors that affect photolysis rates. Additionally, TCEQ requested that ENVIRON investigate methods to improve the speed of the WRFCAMx interface program.

Using a computer program profiler, we determined that the majority of WRFCAMx runtime is spent in input/output (I/O) processes. We were able to reduce runtime by taking advantage of the direct-access capabilities of the WRF netCDF output files. The benefits of this improvement depend significantly on the degree to which data I/O is performed across a network (i.e., network speed/latency, congestion, etc.). Further speed improvements via code parallelization may be helpful to reduce runtime, but the gains would be small relative to the I/O issues described above and so parallelization was not implemented.

We developed an updated KVPATCH program to optionally apply one or more patches to the CAMx vertical diffusivity (Kv) files. A new "OB70" patch replaced the "KV100" technique to enhance low-level mixing in urban areas during nighttime hours. A new cloud patch raises the planetary boundary layer (PBL) when daytime cloud development collapses or suppresses the PBL mixing supplied by the meteorological model (e.g., WRF). The new OB70 and previous KV100 patches yielded comparable ozone model performance against observations. The new cloud patch helped to dilute daytime ozone, and was beneficial in areas where ozone was over predicted in the presence of clouds. The performance impacts from the cloud patch are entirely dependent on the ability of the meteorological model to generate proper cloud distributions.

We tested modifications to the PiG growth algorithm to reduce nighttime puff growth rates consistent with aircraft-measured plume widths at 2-3 hour transport times. Properly simulating plume growth under such conditions is central to the proper characterization of plume chemistry and impacts on next-day ozone. These modifications led to a significant increase in the number of puffs overnight and in turn the largest and most frequent impacts to surface ozone between midnight and noon each day (typically ±10 ppb). Plume differences rarely coincided with monitoring sites in east Texas, resulting in no significant change in statistical model performance. A single obviously faulty PiG-induced ozone impact of 100 ppb occurred on one day in an unmonitored area of Texas. Given the severity of this event, and our current lack of understanding of the mechanism that caused it, we have chosen not to adopt these PiG changes in CAMx at this time. We recommend additional in-depth investigation and potentially other improvements to the PiG algorithm to eliminate such chemically unrealistic PiG behavior.

Finally, we investigated the influence of several environmental factors on photolysis rates and developed an efficient method to represent temperature and pressure dependencies within CAMx for four species: NO_2, O_3, HCHO, and CH_3CHO. Photolysis rate dependencies on temperature and/or pressure were found to be small, as were resulting surface ozone impacts.

We conclude that the efficient parametric method implemented in CAMx to account for these factors is appropriate to the magnitude of the impacts. This approach is far more efficient than the alternative approach of "in-line" computation of photolysis rates by a model such as TUV embedded within CAMx. In addition, the next version of CAMx (v6.00) and its attendant TUV pre-processor will explicitly account for terrain elevation in the calculation of photolysis rates (this change was reserved for CAMx v6.00 because it substantially changes several input file formats).

1.0 INTRODUCTION

The TCEQ uses the Comprehensive Air quality Model with extensions (CAMx), driven by meteorology from the Weather Research and Forecasting (WRF) model, to simulate the chemical reactions, dispersion and fate of ozone and precursors. Photochemical modeling relies upon a wide array of input data that are prepared by computer programs termed "pre-processors." The photochemical modeling system comprising CAMx and its pre-processors is central to State Implementation Plans for Texas' ozone non-attainment areas.

Previous work supported by the TCEQ has identified several areas of improvements related to the vertical mixing, treatment of point source plumes, and representation of chemical reaction rates that depend directly on sunlight (photolysis rates). An optional CAMx pre-processor called KVPATCH is often employed to adjust vertical diffusion inputs to improve the turbulent coupling between the surface and the lower boundary layer. The CAMx Plume-in-Grid (PiG) sub-model is used to treat the physical and chemical evolution of emission plumes from large NOx point sources when they are narrower than the CAMx modeling grid. Photolysis rates for specific gas-phase reactions in CAMx are developed using the Tropospheric Ultraviolet and Visible (TUV) radiative transfer model as a pre-processor.

1.1 Purpose

The purpose of this project was to improve the quality of TCEQ's photochemical modeling for Texas using CAMx by improving the treatment of vertical mixing, refining nocturnal plume growth rates within the PiG sub-model, and accounting for environmental factors that affect photolysis rates. Specifically, we implemented new algorithms into the KVPATCH program to address nighttime conditions in the stable surface boundary layer and cloudy conditions within the daytime boundary layer; updated the PiG with nighttime-minimum turbulence and length scale parameters based on comparisons to nocturnal plume measurements; added a user-controlled flag to apply or ignore wind shear effects on the growth rates of PiG puffs; and added temperature and pressure dependence to photolysis rates for ozone, nitrogen dioxide, and aldehydes. CAMx sensitivity tests were conducted to analyze the effects of each modification relative to unmodified CAMx runs, and to compare to ozone and NOx measurements as available and where feasible.

As an additional task element, TCEQ requested that ENVIRON investigate methods to improve the speed of the WRFCAMx interface program, which translates WRF meteorological data to the input formats required by CAMx.

2.0 WRFCAMX EFFICIENCY IMPROVEMENTS

ENVIRON has analyzed the WRFCAMX meteorological interface program for potential areas of improvement with respect to runtime speed. We applied a FORTRAN performance profiler to determine areas of the program that take the longest to execute. Based on results from the analysis, we considered methods to reduce run time, and were able to improve upon the program's efficiency by taking better advantage of the direct-read access of the WRF output files. This task was also to consider memory management, but upon reviewing the code, we found no areas of redundancy or wasted/unused array space (i.e., no ways to significantly reduce the memory image). The Fortran90 code utilizes dynamic memory allocation that conforms the multi-dimensional array space to the actual grid sizes to be processed.

2.1 Approach

This work started from WRFCAMx v3.2, posted to www.camx.com in October 2011. As primarily a data reformatting interface between the WRF meteorological and CAMx photochemical models, WRFCAMx is an I/O-intensive program, and therefore its speed is dependent on system conditions outside of its control (e.g., disk read/write speed, network latency, etc.).

The most obvious area of improvement that we identified at the start of the project was to take advantage of the WRF netCDF direct-access file structure to improve data reading efficiency. WRFCAMx evolved from its predecessor MM5CAMx, which required sequentially stepping through the MM5 Fortran binary output file structure to find and process the desired range of dates/times. This reduces efficiency when many meteorological records are read but skipped. WRFCAMx inherited this sequential reading approach. The first step was to revise the program to directly read only those file records needed for processing.

The next step involved applying the Portland Group FORTRAN Profiler (PGPROF) utility to a WRFCAMx test case. PGPROF provides many options that track program performance to identify areas of optimization. Program performance can be tracked at the routine level and down to individual lines of code; both routine- and line-level profiling were performed on WRFCAMx.

WRFCAMx was configured to process a set of pre-existing WRF output files to generate a single day of CAMx-ready meteorological files. The WRF test dataset was taken from the 2008 WRAP/WestJump project. The WRF run employed a large 36 km grid with 36 vertical layers covering the Regional Planning Organization (RPO) Continental US (CONUS) modeling domain on the standard RPO Lambert Conic Conformal projection. The RPO CONUS domain includes 148×112×24 grid cells. The WRF output files each contained a single day (23 hours) of meteorological fields spanning 12-11 UTC. CAMx data were processed to yield 24 hours of data between 00-24 CST, requiring two daily WRF files to be processed each CAMx day, and 18 hours of data to be skipped on the first WRF file. WRFCAMx options were selected to maximize the processing burden. First, three-dimensional sub-grid cloud and precipitation fields were diagnosed from the output thermodynamic and surface rainfall rate fields; second, the 26-

category Zhang landuse classification was selected; and third, the CMAQ Kv option was invoked because there was no TKE output available on the WRF file.

All WRFCAMx testing was performed on a quad-core 3.2 GHz Intel Xeon Linux workstation (although only a single CPU was employed for this non-parallelized program). Program I/O was performed in two ways: (1) to and from a remote RAID disk system across our gigabit LAN; and (2) to and from a local disk attached to the workstation. At the time of program testing and profiling, network traffic was minimal and no other processes were accessing the target RAID system.

2.2 Results

2.2.1 Reading Direct Access Files

WRFCAMx v3.2 was configured as described above to generate a single 24-hour period of CAMx-ready meteorological data on the RPO CONUS grid. The revised WRFCAMx (denoted v3.3) was configured in exactly the same manner to benchmark speed improvements from utilizing direct-read access of WRF's netCDF output file structure. This means that v3.3 skips the first 18 hours of unneeded data while v3.2 reads through all records sequentially. Results are tabulated in Table 2-1.

Table 2-1. Comparison of execution times between the original and improved WRFCAMx program. Results for network I/O and local I/O cases are shown.

	Network I/O		Local I/O	
Version	**Execution Time**	**v3.3 Change**	**Execution Time**	**v3.3 Change**
WRFCAMx v3.2	168 s	--	70 s	--
WRFCAMx v3.3	156 s	-12 s (-7%)	33s	-37 s (-53%)

The network I/O cases required significantly more time than the local I/O cases, illustrating the time added for network transfer and RAID access for this I/O-intensive program. To ensure that the network I/O results were representative and not impacted by coincident network traffic or other processes accessing the RAID, both versions of WRFCAMx were rerun several times over the course of two days, and the timing of each was found to vary by only several seconds. The direct-access improvement incorporated into v3.3 further reduced runtime for the local I/O case on both an absolute basis (37 seconds vs. 12 seconds) and on a relative basis (53% vs. 7%).

For quality assurance, the output from both versions of WRFCAMx was compared using the Linux "diff" command. There were zero differences between all of the FORTRAN binary CAMx-ready files. There were no differences in the standard output files in terms of statistics (minimum, average, maximum); the only differences between the standard output files were associated with specific changes to WRFCAMx code with respect to informational diagnostics.

2.2.2 Profiler Results

Profiling with the PGPROG utility first addressed v3.3 program speed associated with entire routines. Subsequently, individual lines in each routine were profiled to understand exactly where resources were spent the most. Both network and local I/O cases were profiled.

Use of the profiler slowed WRFCAMx substantially, requiring nearly 300 seconds to complete a 24-hour run in the network I/O case, and just over 100 seconds in the local I/O case. The two major routines comprising the WRFCAMx run include the main driver routine (WRFCAMx) and the WRF reading/processing routine (READWRF). The relative amount of time spent in each is listed below:

	Overall Time	
Processes	Network I/O	Local I/O
Total Time	*298 s*	*107 s*
WRFCAMx	**60%**	**53%**
Write CAMx files	39%	2%
Kv and misc. calculations	9%	17%
Output field statistics	6%	18%
Interpolation/vertical mapping	6%	15%
READWRF	**40%**	**47%**
Units conversion, cloud preparation	17%	21%
Read WRF files	13%	12%
Cloud/precipitation diagnosis	10%	14%

Line-by-line profiling in the network I/O case revealed that the majority of time (39%) spent in the main WRFCAMx driving routine was associated with writing new CAMx FORTRAN binary output files. Writing is usually a much more expensive process than reading, especially on a RAID system as multiple images are created as a means of backup and maintaining data integrity (e.g., preventing data corruption). Reading WRF files required 13% of total runtime, the third-ranked process. Unit conversions and the calculation of additional variables (total pressure from mean and perturbation, layer heights, Kv and cloud/precipitation processing) required 36% of total runtime, the second-ranked process. Interpolation, vertical layer mapping, and statistics of the output fields required 12% of total process time.

In the local I/O case, the time necessary to write CAMx files all but vanished, and WRF reading times were reduced proportionally. Number-crunching routines that are not dependent on I/O, such as mapping, Kv calculations, and statistics, required roughly the same amount of absolute time to process as in the network I/O case, as expected.

The I/O processes are dependent on hardware conditions (CPU speed, network speed/latency/traffic, disk speed), so WRFCAMx cannot be further modified to improve I/O efficiency. Note that TCEQ's experience with WRFCAMx I/O runtimes may vary according to their specific hardware configuration. The efficiency of internal calculations for clouds,

precipitation and Kv may be improved with the use of OMP parallelization. Assuming that each individual loop related to these calculations was parallelized and that OMP parallelization over four processors was 100% efficient (a factor of 4 faster), the total runtime would decrease by a maximum of 27% in the network I/O case and 39% in the local I/O case (OMP overhead would mitigate this speedup).

3.0 VERTICAL MIXING IMPROVEMENTS

ENVIRON has updated the KVPATCH vertical diffusivity pre-processor to improve the nighttime surface layer adjustment and to maintain elevated diffusivities in vertical grid columns where afternoon deep cloud development cools the surface and suppresses or collapses modeled boundary layer depths. We then tested these modifications in CAMx sensitivity runs using a preexisting DFW eight-hour ozone modeling dataset. Results of the modeling sensitivities were analyzed with respect to diffusivity inputs derived using the original KVPATCH program to determine the impact of the modifications.

3.1 Background

Vertical diffusivity (Kv) is a critical input parameter for the CAMx chemical transport model as it controls the rate of vertical turbulent (sub-grid scale) mixing of pollutants among the model layers that comprise the surface and planetary boundary layers (SBL and PBL, respectively). All models like CAMx are very sensitive to vertical mixing because it directly controls surface concentration predictions. The Kv input field is derived by the WRFCAMx interface program from various meteorological parameters that are simulated by the WRF prognostic meteorological model. The specific methodology by which Kv is calculated from WRF output depends on how the PBL is simulated within WRF.

Historically, TCEQ has applied a CAMx pre-processor called KVPATCH that adjusts diagnosed Kv fields by imposing a higher Kv floor in the SBL. This is done to maintain a low intensity of mixing throughout the night and early morning hours to weakly mix surface emissions upward and control over predictions of NOx that otherwise often occur in urban areas. Over predictions of nighttime/morning NOx can lead to complete titration of ozone locally, and to inhibited ozone formation well into late morning hours, and may ultimately impact model performance in replicating observed afternoon peak ozone.

The KVPATCH program applies two different patches within a user-defined SBL depth (usually 100 or 200 m):

1. A landuse-dependent minimum Kv, where for urban areas the floor is set to 1 m^2/s, for forests it is set to 0.5 m^2/s, and for all other classifications it is set to 0.1 m^2/s;
2. A more arbitrary adjustment that sets the minimum Kv for all layers within the SBL to the maximum Kv value found within that depth (often referred to as “KV100” or “KV200”).

This approach has generally served TCEQ’s modeling well. In a previous work order in which ENVIRON implemented alternative Kv calculation methodologies in the WRFCAMx interface (ENVIRON, 2011), it was noted that the (unpatched) OB70 approach maintained elevated Kv values within the overnight SBL, similarly to the KV100 patch (#2 above). Furthermore, it generally resulted in improved overnight performance for NOx and ozone concentrations in the Dallas – Fort Worth (DFW) area relative to the other (unpatched) Kv options (although it was the worst option in replicating midday ozone levels). As a result, OB70 was seen as a more

suitable and defensible approach for Kv patching within the nocturnal SBL than the KV100/200 technique.

As a result of recommendations stemming from that previous work, ENVIRON was directed to (1) implement the OB70 technique within KVPATCH as a replacement of the KV100/200 approach, and (2) expand KVPATCH to address PBL collapses under afternoon convective clouds.

3.2 Approach

Three changes have been implemented in KVPATCH. First, the landuse-dependent patch was retained, but it was slightly modified to set minimum SBL Kv for all non-urban categories to 0.1 m^2/s (i.e., reducing the minimum Kv for forests from 0.5 m^2/s). The minimum SBL Kv for the urban category was retained at 1 m^2/s.

Second, we replaced the current KV100/200 patch with the OB70 (O'Brien, 1970) profile methodology. The OB70 algorithm is used to set the minimum SBL Kv profile for any grid columns containing a non-zero urban landuse fraction. There are three inputs to OB70: mixing depth, Kv in the first layer, and Kv at the top of the mixing depth. As in the previous KVPATCH, the user defines the depth over which to apply the OB70 patch (e.g., 100 or 200 m), and that is used for the first OB70 input, "mixing depth". The second input, Kv in the first layer, is set to the input Kv value in layer 1 after the landuse-weighted patch is applied. The third input, Kv at the top of the mixing depth, is set to a constant value of 1 m^2/s. For urban grid cells, this typically sets nocturnal SBL Kv values to ≤5 m^2/s.

We then added a third (new) patch to handle convective cloud activity. The original idea for this patch was to maintain elevated Kv values within vertical grid columns where thick convective cloud develop during the midday, cool the surface, and cause the modeled planetary boundary layer (PBL) to rapidly collapse. In the past, this phenomenon was common when the MM5 meteorological model was run with simplistic bulk PBL parameterizations as opposed to more advanced schemes (e.g., TKE). It remains unclear whether WRF consistently suffers from the same symptoms when newer bulk PBL schemes like YSU are used. Nevertheless, our original approach considered maintaining consistency and persistence in the Kv profiles in a spatial and temporal sense; i.e., based on nearby grid column values over similar landuse types, and/or based on the previous hours before the collapse occurred.

In order to test the new convective patching scheme, we attempted to identify an area/period in the TCEQ June 2006 Rider 8 modeling dataset with strong cloud-related PBL collapses. We screened the evolution of CAMx PBL and cloud fields simultaneously over the 12 and 4 km grids. While plenty of convective activity occurred throughout June 2006, we found that the WRF/YSU run very rarely developed conditions where afternoon convective cloud development caused the PBL to prematurely collapse toward the SBL.

We decided to expand this patch to incorporate diffusive mixing beyond the PBL through the entire overlying cloud depth. The patch was re-designed to identify those grid columns

containing cloud cover with a base below or near the PBL top, and to extend the Kv profile to the cloud top using the OB70 technique. The screening for cloud-induced reductions of PBL depths was retained. In this way, surface-based turbulent mixing would more appropriately extend into and within the clouds, mimicking the effect of a convective cloud model. The same three OB70 input parameters are required; in this case the "mixing depth" is set to the top of the convective cloud, the layer 1 Kv (reflecting patches 1 and 2) is used, and the Kv at the top is set to 1 m^2/s. This results in potentially large Kv profiles extending rather deep through the troposphere, but limited only to grid columns containing daytime convective cloudiness. At night, the PBL drops to the SBL and separates from remaining cloud bases, thereby switching this patch off.

Figure 3-1 shows an example of the cloud patching effect for a particular grid column. Diffusivity profiles were extracted at 1300 CST on June 20, 2006 for a 4-km grid column over south-central Texas. The "no-cloud" Kv profile reflects the first two patches (landuse-dependent SBL minimum and the OB70 SBL minimum) but does not include the cloud patch. The PBL depth at this hour was diagnosed to be about 700 m after peaking an hour earlier at over 1300 m. The no-cloud Kv profile was accordingly shallow and weak, peaking at only 5 m^2/s, and it is obvious that the PBL in this grid column was influenced by the buildup of afternoon cloudiness. The cloud base and top in this grid column was 1000 m and 4000 m, respectively. While the cloud base was 300 m higher than the PBL depth, the cloud patch compares the PBL to the non-cloudy over-land average PBL for this hour (~1300 m) and uses that to account for a potentially cloud-induced shallow PBL. The new effective PBL was set to the 4000 m cloud top and OB70 was used to calculate a revised Kv profile. The new Kv peak was 60 m^2/s at an altitude of about 1500 m.

Figure 3-2 compares the diagnosed PBL derived from pre- and post-adjusted Kv fields over the 4 km grid for the same time as Figure 3-1. Also shown is the horizontal distribution of the cloud field at the same time, expressed as cloud optical depth. Some increases in PBL depth are significant, reaching up to 9000 m in the deepest convective towers in the north-central portion of the state. Peak Kv values in such columns reach well over 1000 m^2/s at about 5000 m.

3.3 Modeling Results

Three CAMx runs were performed to evaluate ozone and NOx sensitivity to the Kv patches. All runs used inputs obtained from TCEQ for the Rider 8 May 31 – July 1, 2006 episode. TCEQ developed meteorology using WRF with the YSU PBL scheme, and configured CAMx version 5.40 to use the Zhang dry deposition scheme. TCEQ applied the original version of KVPATCH to the CAMx-ready vertical diffusivity input fields, which included the landuse and KV100 patches. The CAMx "KV100" run described below represents our base case, and is configured exactly like the TCEQ base run except that the plume-in-grid feature was not used. Our "OB70" run had the same configuration, but applied the revised landuse and OB70 patches; the "OB70+CLD" run added the cloud patch on top of the revised landuse and OB70 patches.

Figure 3-3 displays ozone differences over the 12 km domain at noon, 6 PM, and 9 PM on June 20. Widespread ozone reductions in the OB70 run occurred mainly at night relative to the

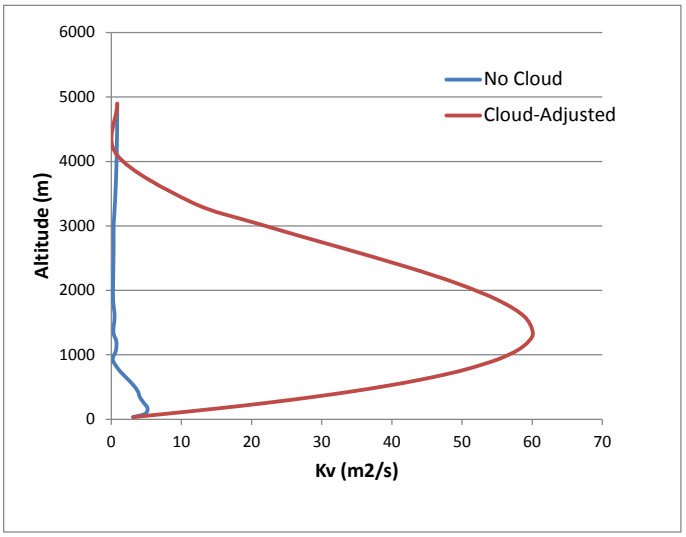

Figure 3-1. Kv profiles at 1300 CST, June 20, 2006 for a 4-km grid column over south-central Texas. The pre-adjusted Kv profile (blue) indicates shallow/weak mixing; the adjusted profile (red) accounts for mixing through the cloud depth.

KV100 run (left plots) because: (1) the OB70 patch only applies to urban areas whereas the KV100 patch was applied everywhere; and (2) the landuse patch was modified in the OB70 case to revert minimum Kv's over forests back to 0.1 m^2/s. Impacts from the cloud patch occurred during the daytime (right plots) as it increased mixing where convection built up and caused PBL depths and Kv profiles to otherwise collapse.

Four sites in Texas where both ozone and NOx observations were collected in 2006 were used to evaluate the sensitivities to the Kv patches -- Hinton (Dallas), Pecan Valley (San Antonio), Houston East (Houston), and Longview (Northeast Texas). Time series of surface layer hourly ozone and NOx at Hinton are displayed for the first 10 days of June (Figure 3-4); patterns for the remainder of the month are similar.

Near-surface Kv values tended to be larger for the KV100 patch than for OB70, but this did not appear to affect the daytime ozone peaks, indicating that the unpatched daytime Kv's were already large enough to provide sufficient low-level mixing. The OB70+CLD patch generally raised the collapsed PBL depth during the afternoon on some dates, resulting in higher vertical diffusivities in most PBL layers and mixing out some of the ozone. In the evening, the KV100 patch kept near-surface Kv's over Hinton the same or higher than either the OB70 or OB70+CLD. The increased mixing helped ventilate more NOx out of layer 1, slowing the ozone titration and agreeing better with both ozone and NOx observations, particularly on the evenings of June 4 and 5.

Figure 3-5 compares hourly vertical Kv profiles over Hinton from 5 to 10 PM on June 15. The cloud patch made no impact during this period. At 5 PM, all scenarios were well mixed. By 6

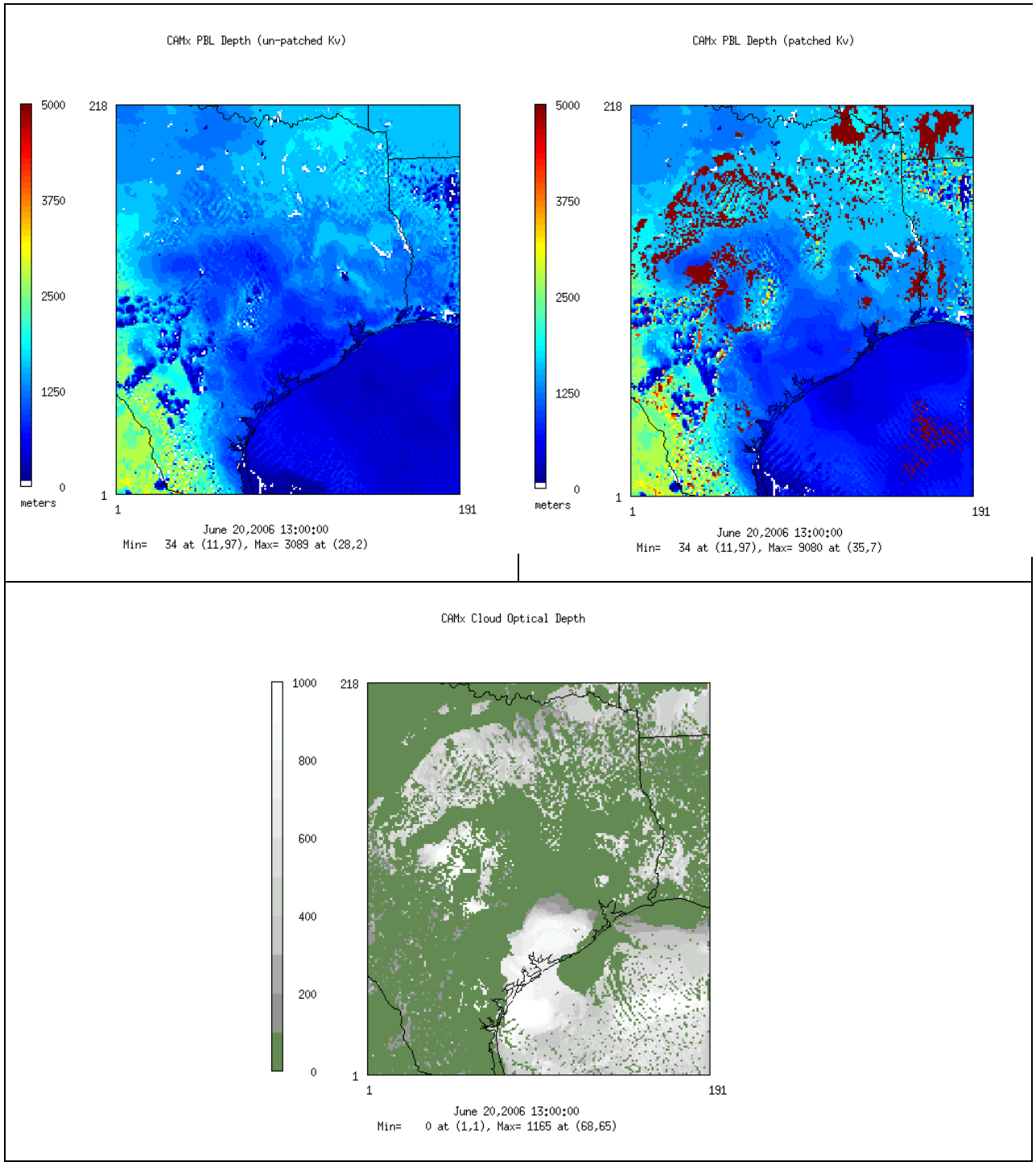

Figure 3-2. PBL fields at 1300 CST, June 20, 2012 on the TCEQ Rider 8 4 km modeling grid derived from the un-patched (upper left) and patched (upper right) Kv fields. CAMx cloud field as optical depth (bottom) is shown for reference.

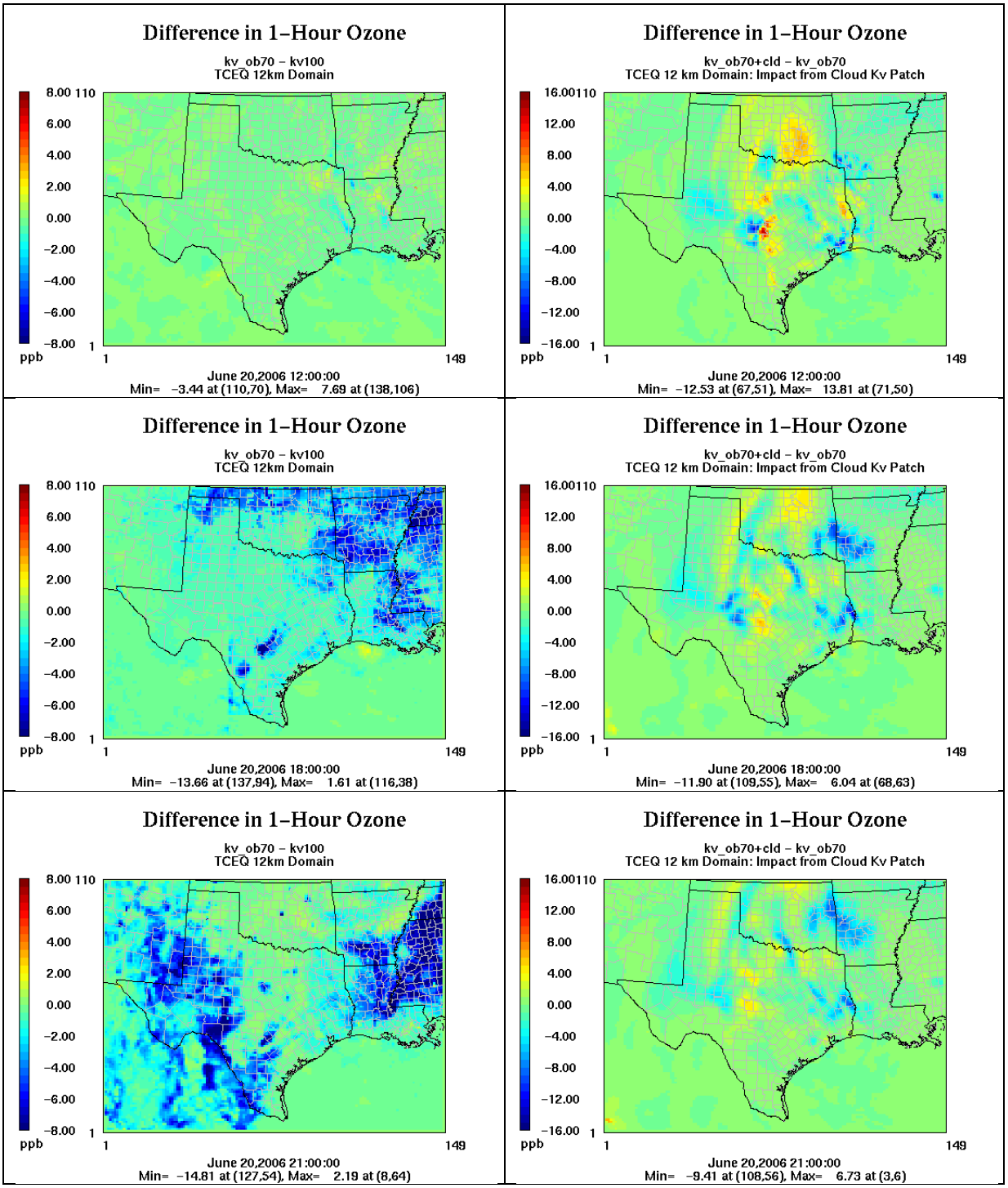

Figure 3-3. Ozone difference plots at noon, 6 PM, and 9 PM on June 20, 2006 over the 12 km CAMx modeling domain. Plots on the left show the differences caused by the introduction of the OB70 patch relative to the KV100 run; plots on the right show the differences caused by the introduction of the cloud patch relative to the OB70 run.

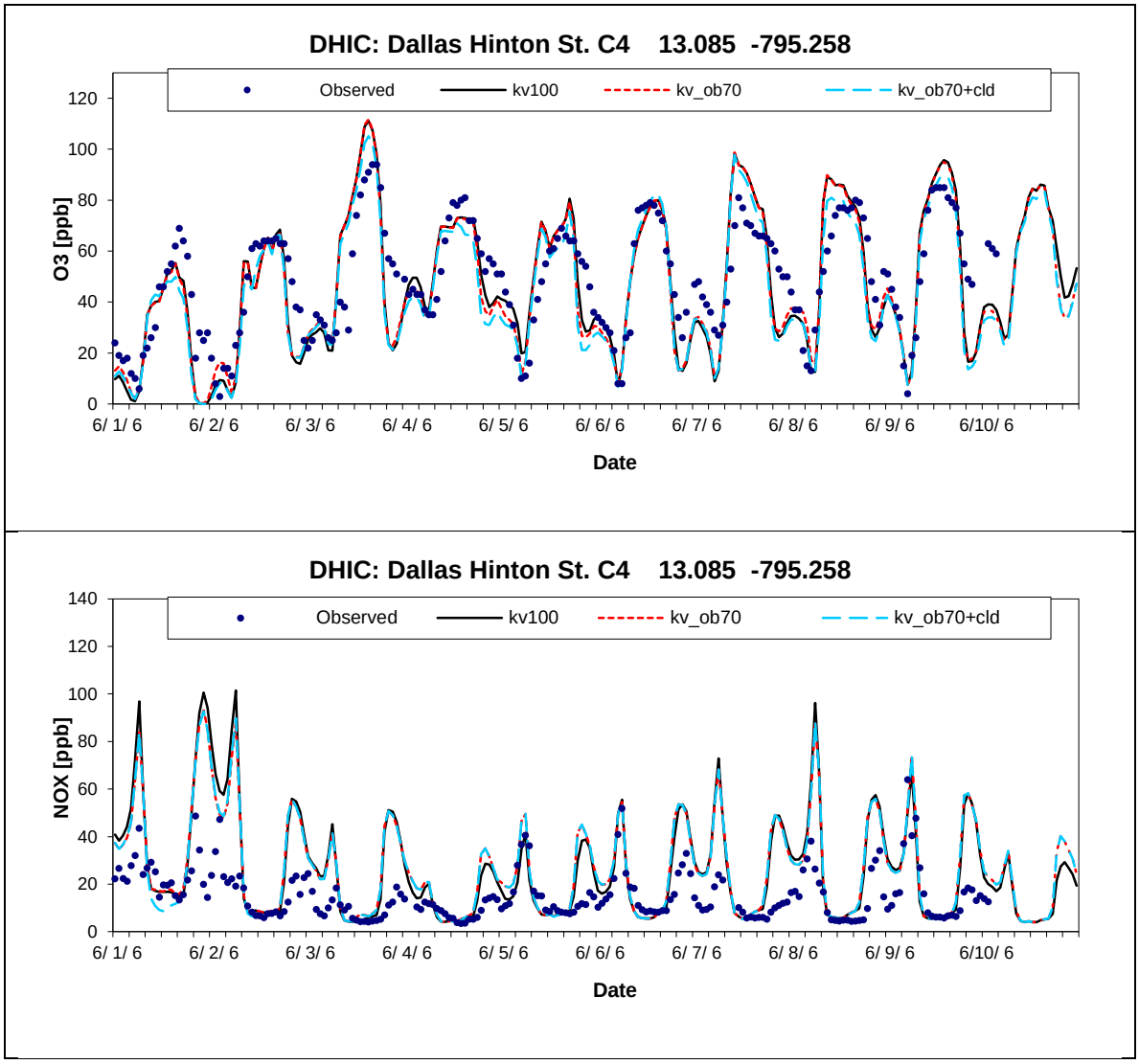

Figure 3-4. Hourly time series at Hinton of observed and CAMx simulated ozone (top) and NOx (bottom) during June 1-10, 2006. Blue dots are measurements, black line is the KV100 run, red dashed line is the OB70 run, and blue dashed line is the OB70+CLD run.

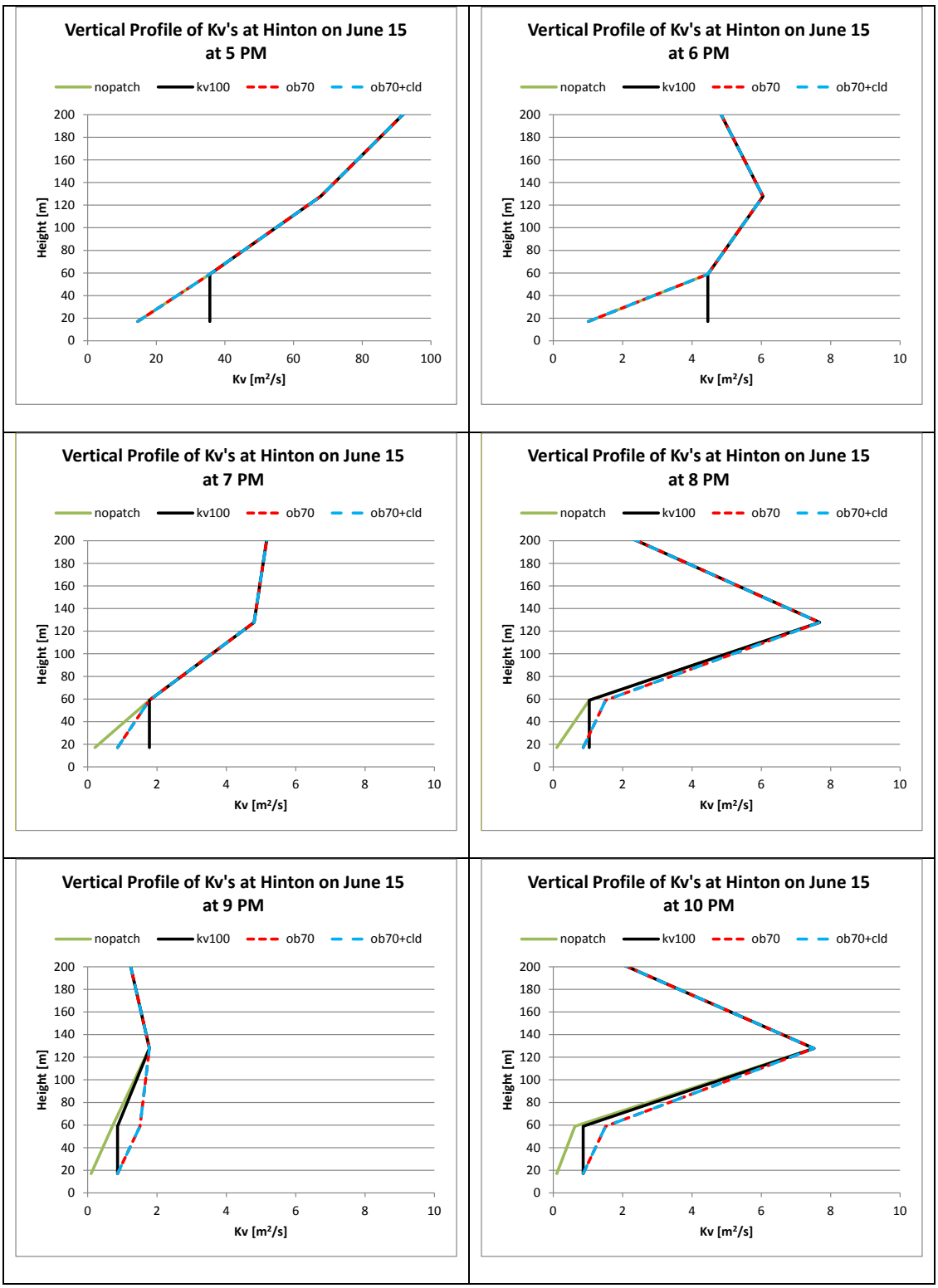

Figure 3-5. Hourly vertical Kv profiles at Hinton on the evening of June 15, 2006. Color assignments are the same as in Figure 3, but a "no patch" profile is added in green. Note x-axis scaling is different on the 5 PM plot.

PM, Kv's dropped by an order of magnitude; the KV100 patch boosted near-surface Kv's more than the other patches, helping to mix out some NOx emissions and slow down ozone titration. By 9 PM, all near-surface Kv's were assigned to the minimum value; the OB70 and OB70+CLD patches generated higher Kv's in layers 2 and 3 than the KV100 patch. This pattern occurred on several dates, as the KV100 patch produced the same or higher layer 1 Kv's for most of the night while the OB70 patch produced higher Kv's in layers 2 and 3 after sunset.

Time series of ozone and NOx at Houston East, Pecan Valley, and Longview are shown in Figure 3-6 through Figure 3-8. The patterns were similar to Hinton. At night, the KV100 patch always generated the same or higher near-surface Kv's than either OB70 or OB70+CLD cases. As a result, over predicted NOx was reduced more during the evening hours when using the KV100 patch than OB70, but it did not translate into much change for ozone. All three sites exhibited reductions in daytime peak ozone in the OB70+CLD run on some days, particularly in Houston and Longview. Generally these reductions led to improved performance toward the observations.

Figure 3-9 shows time series of the hourly Kv profiles over Longview from 10 AM to 2 PM on June 2 when midday clouds drifted over the grid cell, and on June 7 when deep convection occurred in the area. The top plot shows the Kv profiles before being patched; the bottom plot shows the resulting OB70+CLD patch. The 12 PM Kv profile is highlighted in red. On June 2 the 12 PM profile exhibits much lower PBL and Kv values relative to the profiles in the surrounding hours. Very little differences are seen among the June 7 profiles, suggesting no deep clouds existed within this particular grid column. Table 3-1 lists the hourly PBL depths over Longview on both days in the unpatched case; the PBL depth was cut nearly in half at 12 PM on June 2 but little effect is seen on June 7. The OB70+CLD patch raised the PBL at 12 PM on June 2, and the Kv profile was enhanced throughout the revised PBL. The PBL depths and Kv's at 10 and 11 AM were also elevated due to the cloud patch. The OB70+CLD patch resulted in little difference in PBL mixing on June 7.

Figure 3-10 presents a blowup of the Longview ozone time series on June 2 and 7 that compares the OB70 and OB70+CLD results. Note that on June 2 the modeled ozone concentrations began to drop or hold steady between 9 AM and 12 AM while observed ozone did not show a dip in ozone until 1 PM, suggesting that modeled clouds may have passed over Longview too early in the day. On June 7, clouds developed and propagated from east to west beginning around 10 AM (Figure 3-11). The OB70+CLD run resulting in very good agreement with observations after 11 AM, which suggests that ozone was diluted upwind before being transported to Longview. Although the OB70+CLD patch helped increase vertical mixing within the PBL and reduce midday ozone over predictions on several days, the success of this patch is highly dependent on good meteorological inputs.

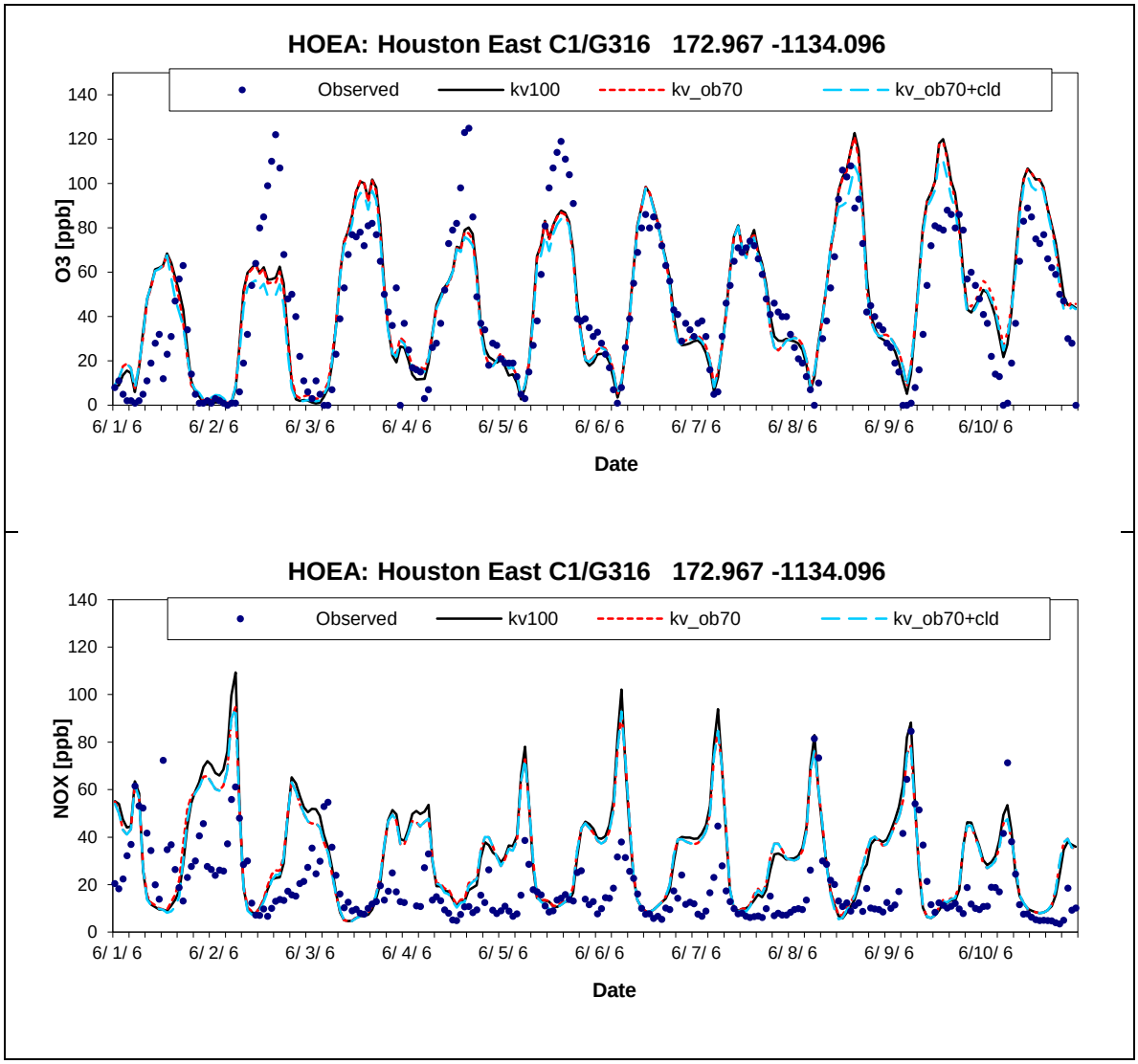

Figure 3-6. Hourly time series at Houston East of observed and CAMx simulated ozone (top) and NOx (bottom) during June 1-10, 2006. Blue dots are measurements, black line is the KV100 run, red dashed line is the OB70 run, and blue dashed line is the OB70+CLD run.

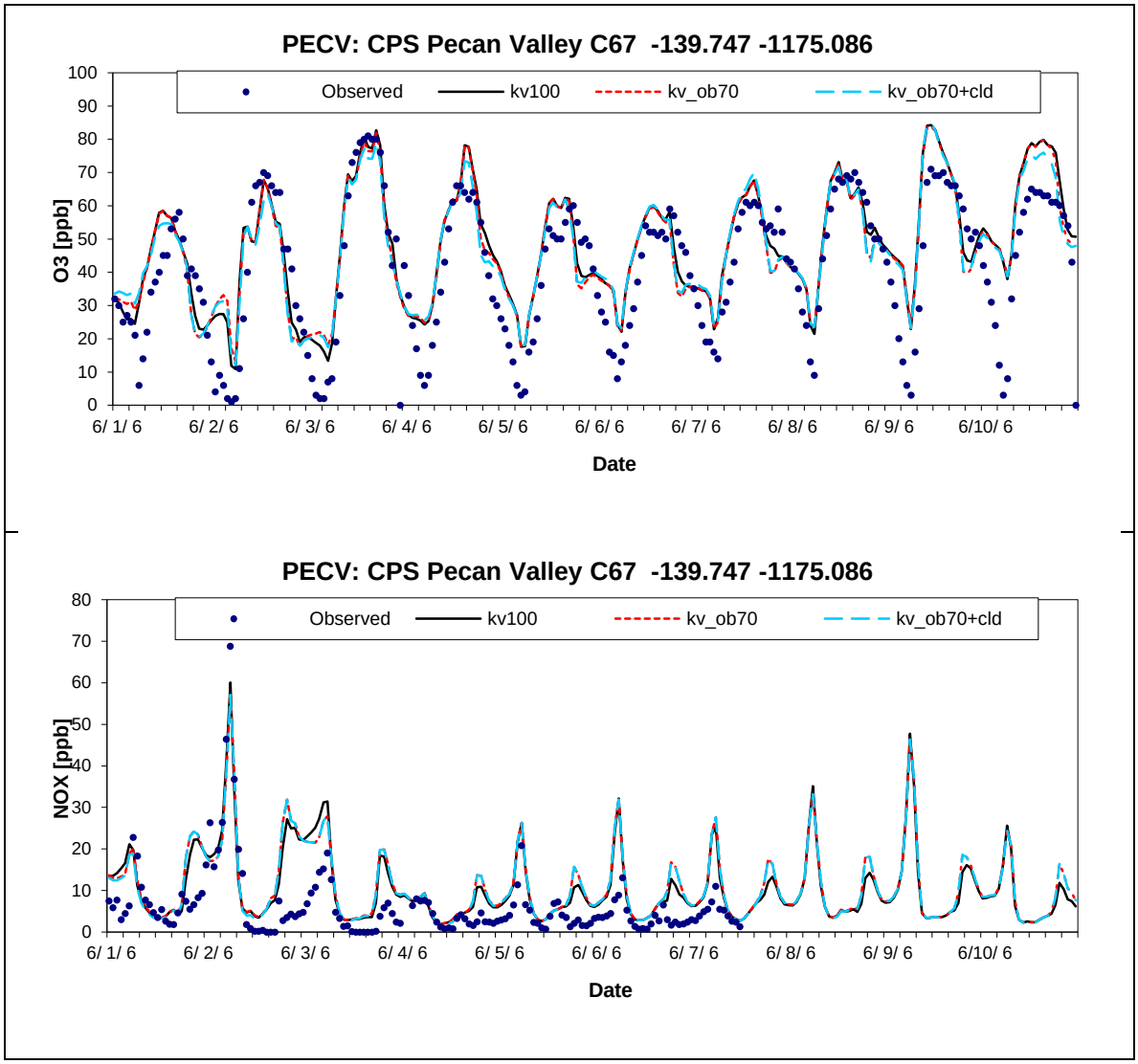

Figure 3-7. Hourly time series at Pecan Valley of observed and CAMx simulated ozone (top) and NOx (bottom) during June 1-10, 2006. Blue dots are measurements, black line is the KV100 run, red dashed line is the OB70 run, and blue dashed line is the OB70+CLD run.

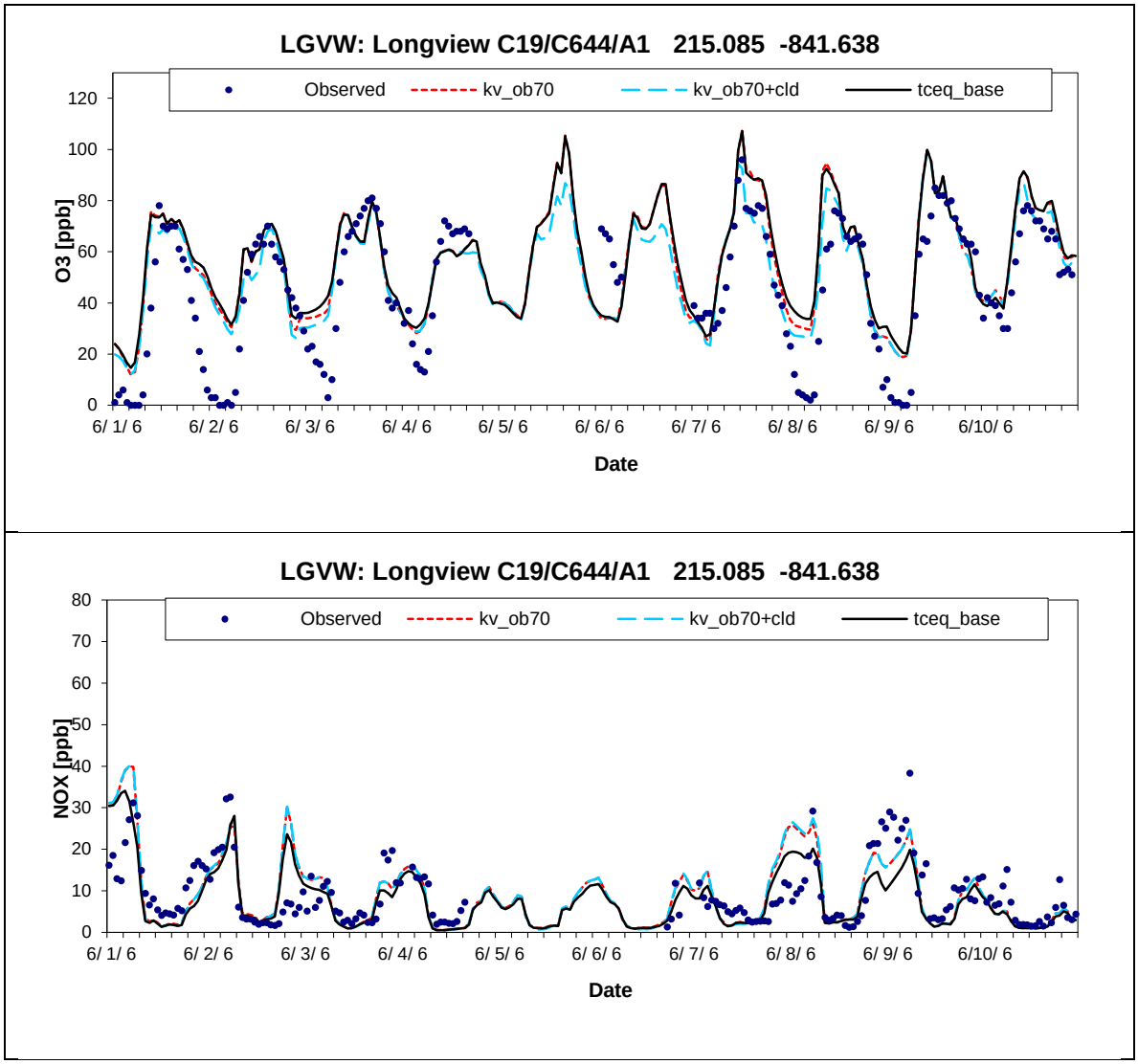

Figure 3-8. Hourly time series at Longview of observed and CAMx simulated ozone (top) and NOx (bottom) during June 1-10, 2006. Blue dots are measurements, black line is the KV100 run, red dashed line is the OB70 run, and blue dashed line is the OB70+CLD run.

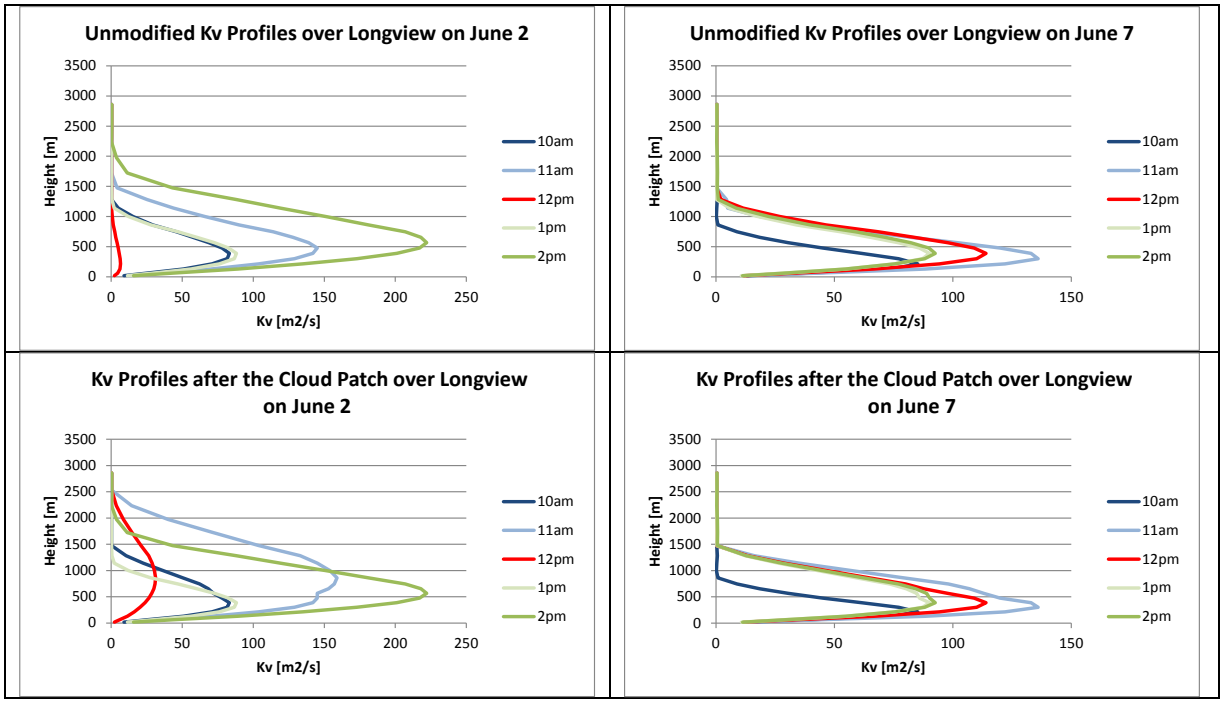

Figure 3-9. Time series of Kv profiles over Longview on June 2 (left) and June 7 (right), before (top) and after (bottom) applying the cloud patch.

Table 3-1. Simulated PBL depths over Longview on June 2 and 7 according to unpatched Kv inputs.

Hour	PBL [m] on June 2	PBL [m] on June 7
8 AM	430	256
9 AM	1060	520
10 AM	1210	930
11 AM	1590	1210
12 PM	795	1360
1 PM	1210	1220
2 PM	1850	1360

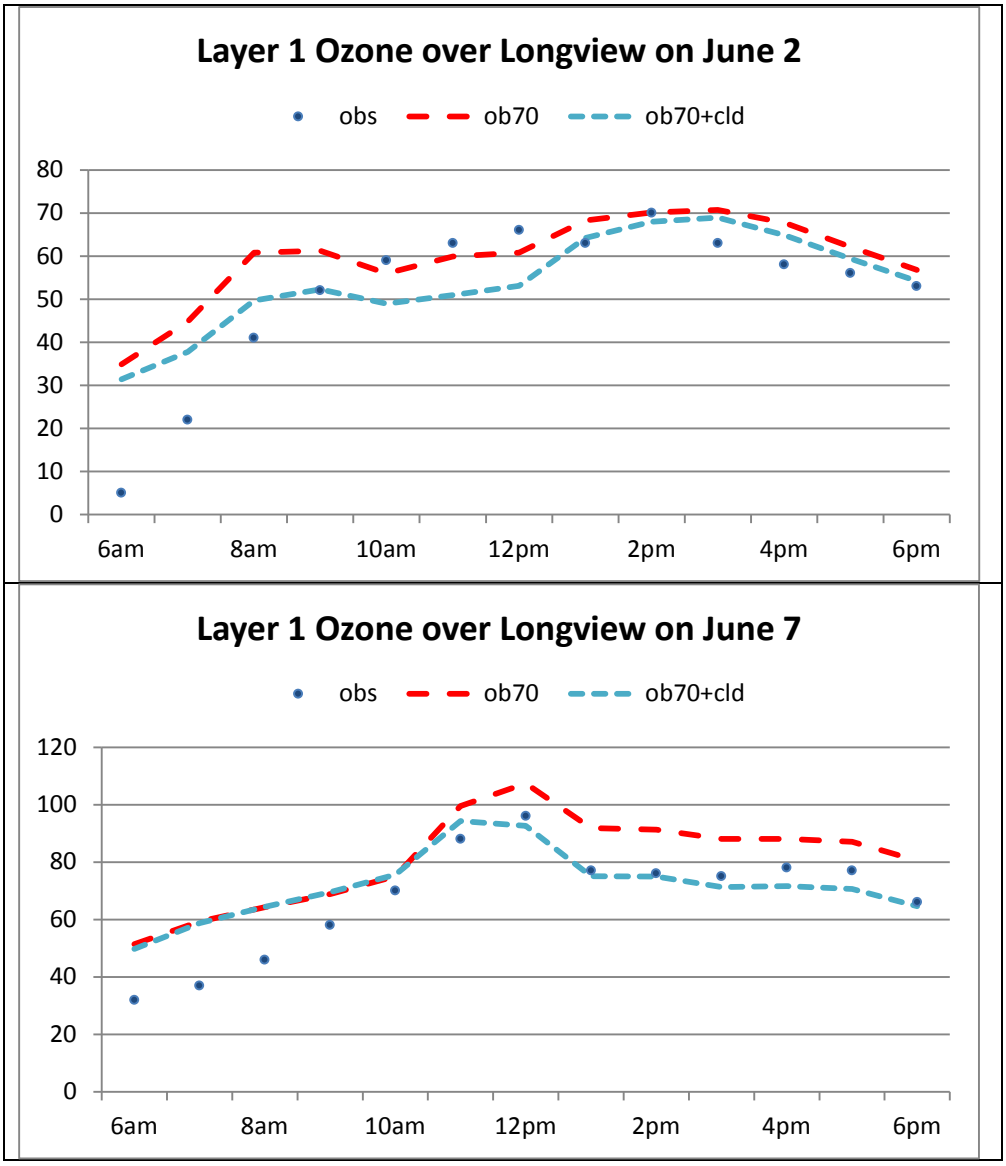

Figure 3-10. Time series of observed and simulated hourly ozone on June 2 at Longview. The blue dashed line shows the impact of the cloud patch.

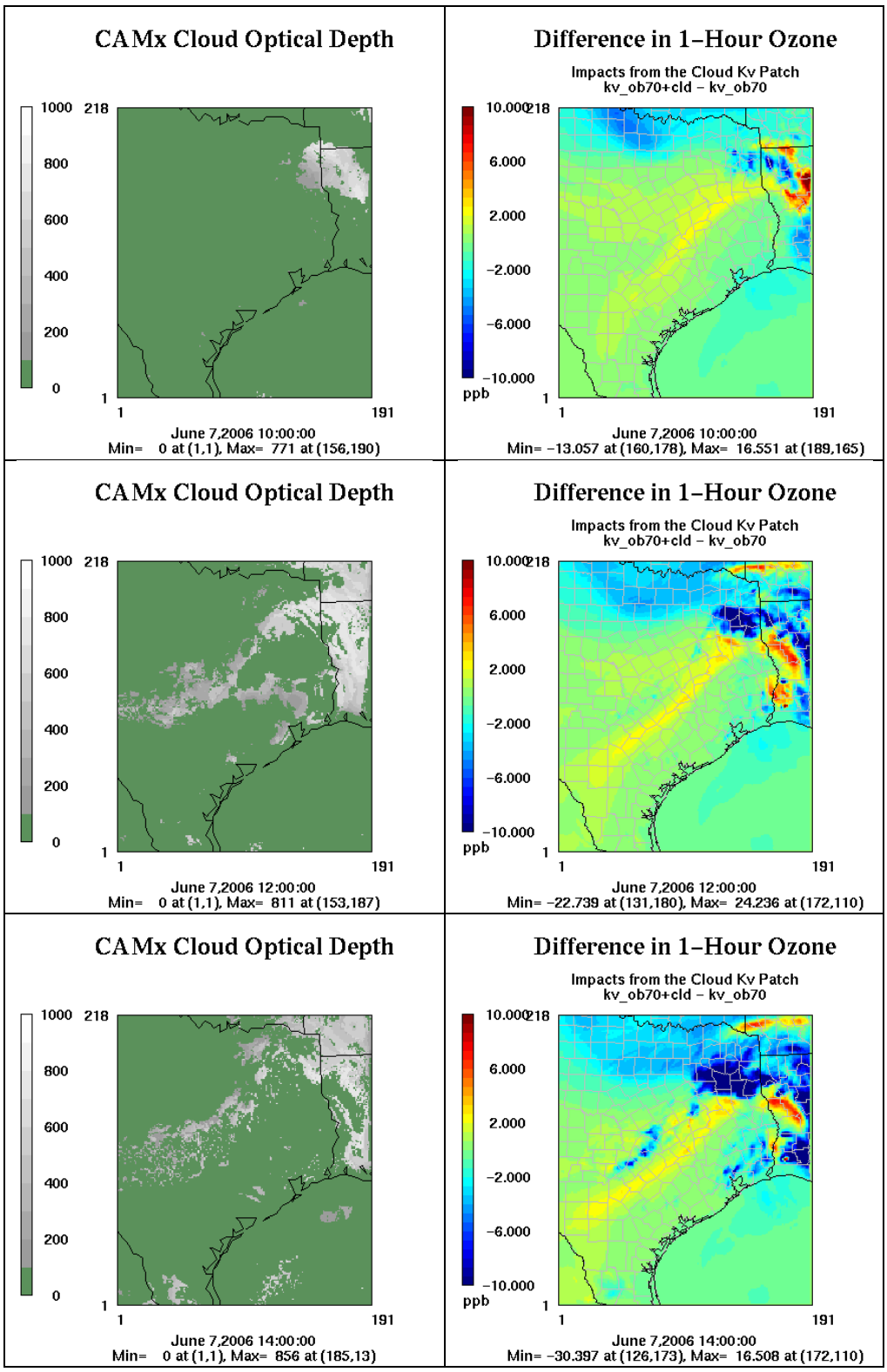

Figure 3-11. Cloud optical depth (left) and ozone differences (right) caused by the cloud patch on June 7 at 10 AM, 12 PM, and 2 PM.

3.3.1 Statistical Performance in DFW

Ozone model performance from the three CAMx runs was evaluated in the Dallas/Fort Worth area to help quantify the impacts of the updated Kv patches. Figure 3-12 and Figure 3-13 show daily ensemble statistics (paired peak accuracy, normalized bias and gross error) for 1-hour ozone from 19 DFW ozone sites. Statistics were calculated for hours when observed ozone was at least 40 ppb.

The peak accuracy statistics using the KV100 and OB70 patches were similar on most dates even though the KV100 patch was applied throughout the domain and the OB70 patch was limited to urban cells. Again, these patches were designed to impact model performance at night, when observed ozone decreases well below 40 ppb. Indeed, most differences between these runs occurred at night (Figure 3-3). In both runs, CAMx tended to over predict the 1-hour ozone peaks on most dates. The OB70 patch occasionally and marginally reduced the peak bias. Peak ozone performance was more impacted by the OB70+CLD patch, with less positive (more negative) paired peak accuracy. Since most dates exhibited a positive bias in DFW, the OB70+CLD run tended the show the best performance.

Overall, the KV100 patch tended to yield the highest normalized bias, while the OB70+CLD run had the lowest bias. The latter performed exceptionally well on June 8 and 23, bringing the normalized bias within the 15% target range. Similarly, the OB70+CLD run exhibited the best gross error performance, especially for June 3, 7–8, and 20–24.

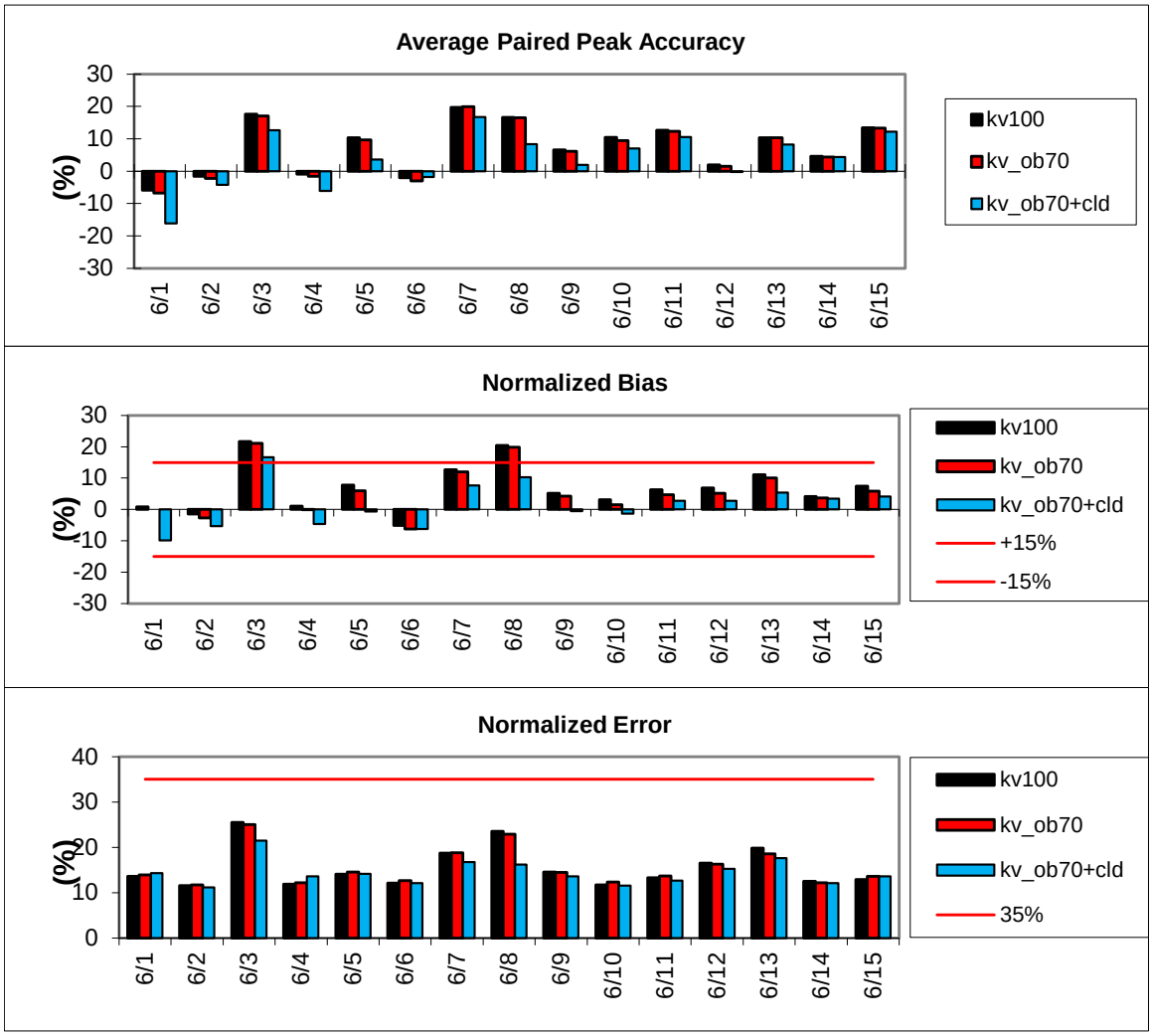

Figure 3-12. Daily model performance statistics for 1-hour ozone over 19 sites in DFW, June 1-15, 2006.

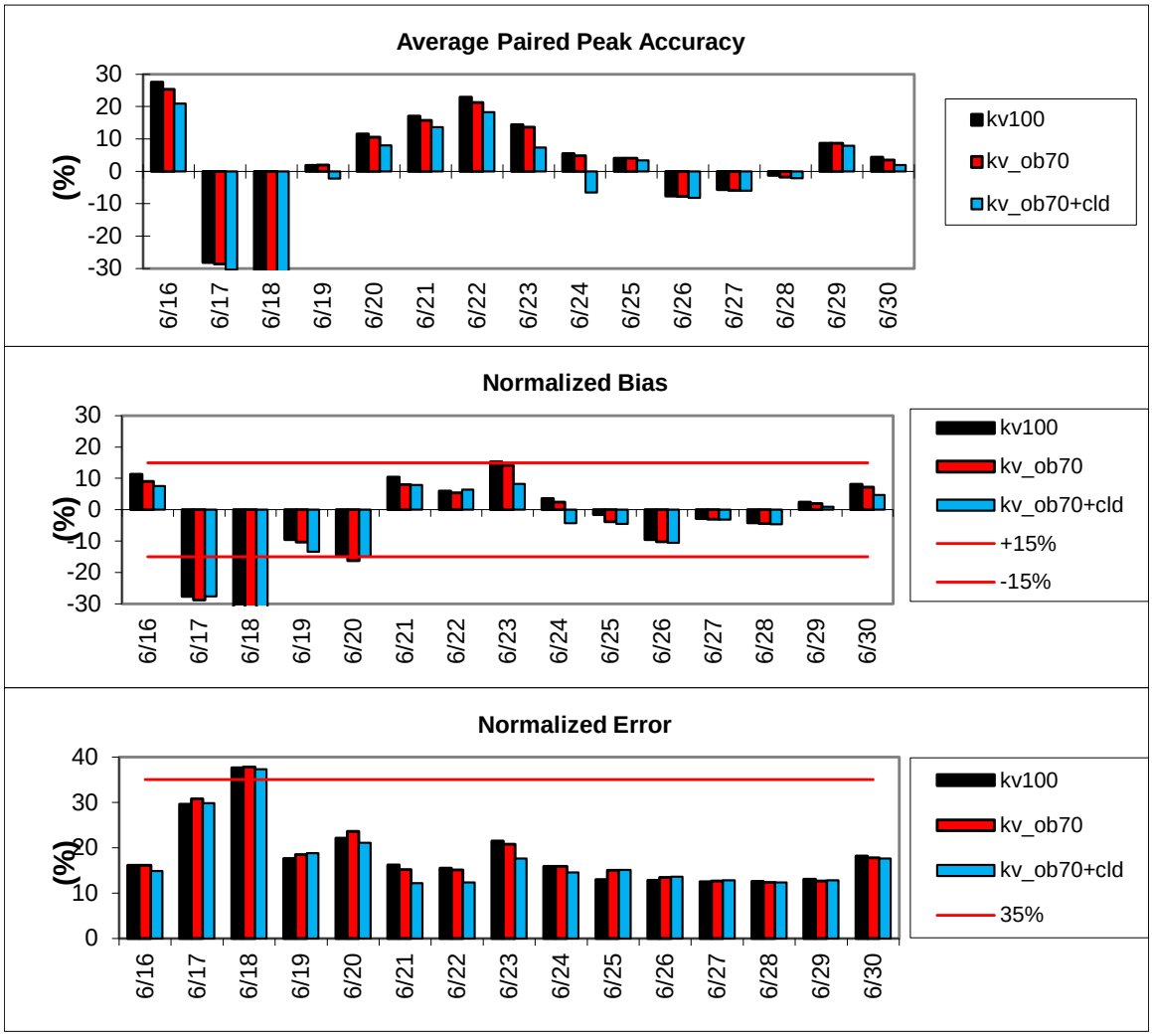

Figure 3-13. Daily model performance statistics for 1-hour ozone over 19 sites in DFW, June 16-30, 2006.

4.0 MODIFICATIONS TO PIG NIGHTTIME GROWTH RATES

This task addresses recommendations stemming from the analysis of nighttime plume dispersion performed under Project 10-020 (Yarwood et al., 2012) of the Texas Air Quality Research Program (AQRP). We modified the PiG module to reduce nighttime puff growth, specifically targeting parameters defining the free atmosphere turbulent length scale and minimum turbulent energy. We also added a switch to the CAMx PiG option that allows the user to apply or ignore the effects of explicit wind shear on plume growth rates. We then tested these modifications in CAMx sensitivity runs using a preexisting DFW ozone modeling dataset. Results of the modeling sensitivities were analyzed with respect to the unmodified version of CAMx to determine the impact of the modifications.

4.1 Background

Yarwood et al. (2012) compared CAMx simulations employing several PiG configurations and a super-high resolution (200 m) flexi-grid against aircraft measurements recorded during multiple transects through the Oklaunion power plant plume on the night of October 10, 2006. Yarwood et al. used CAMx v5.30 for all simulations. Plume widths from the flexi-nested run and aircraft measurements were expressed as a "full width at half maximum" (FWHM) metric, which is roughly equivalent to $\pm 1\sigma$ from plume centerline (2σ total width) of a Gaussian distribution. PiG puff widths and depths, on the other hand, extend $\pm 1.5\sigma$ from the puff centerline (3σ total width). For clarity and consistency, all plume widths in this document are given as FWHM.

The first PiG case run by Yarwood et al. placed the Oklaunion nighttime plume at about the correct altitude with about the correct depth. However, lateral plume spread was too large, exceeding 3 km within 1 hour downwind and reaching 13 km by 2 hours. Aircraft transects at similar downwind distances suggested plumes no wider than 1-2 km. The simulated plume on the 200 m flexi-nested grid performed better; it was roughly 1 km wide within 1 hour downwind and slowly grew to 3-5 km wide between 2-3 hours. However, flexi-nesting took 168 times longer than PiG to run a 6 hour period.

By removing the contribution from explicit (grid-resolved) wind shear on puff growth rates and lowering the nighttime minimum values for vertical turbulent mixing, Yarwood et al. found that PiG plume widths were reduced to 3-6 km out to 2 hours, consistent with the flexi-nested run. Additional ad-hoc reductions, including cutting horizontal growth rates by 50% and zeroing vertical growth rates, constrained puff depths to less than 100 m and puff widths to 2-3 km between 1 and 2 hours downwind.

The modeling described by Yarwood et al. demonstrated the importance of properly characterizing plume dimensions with respect to downwind impacts on next-day ozone. Excessive growth rates lead to over dilution of emitted NOx, excessively rapid reactions with ozone and associated NOz generation overnight, early transfer of plume mass to the grid, and diminished impacts on next-day ozone. As a result of that AQRP work, CAMx v5.40 was publicly released with certain PiG modifications: (1) no explicit shear-induced puff growth during nighttime/stable conditions, (2) minimum puff vertical diffusivities reduced to 0.1 m^2/s, and (3)

nighttime stable residual layer reduced from 1000 m to 100 m. Recommendations stemming from that work included adding a user-defined flag to turn off explicit shear growth at all times, and investigating minimum horizontal turbulent energy and length scales in stable environments. These recommendations are the subject of the modifications described below.

4.2 Approach

CAMx v5.40 was modified with a new PiG control switch located with the other PiG configuration variables in the CAMx parameter file (`Includes/camx.prm`). The switch is called SHRFLG, and it controls whether and how explicit (grid-resolved) horizontal and vertical shear measured across the puff dimensions is used in the puff growth equations:

`SHRFLAG = 0`	Shear is never applied
`SHRFLAG = 1`	Shear is applied during neutral/unstable conditions only
`SHRFLAG = 2`	Shear is always applied

Horizontal puff growth during stable conditions was further analyzed for several alternative configurations with the intent of further reducing plume dimensions over 2-3 hour transport times. No additional modifications to vertical puff growth were considered; this decision was based on results from Yarwood et al. (2012) showing that vertical plume dimensions were consistent among PiG, flexi-nest, and aircraft observations.

Changes to the puff growth module were tested outside of CAMx by running it within a separate driver program to simulate the time evolution of one puff under an idealized stable nighttime environment, during which time the minimum defaults for free-atmosphere turbulent length scale and turbulent energy were applied. Since the height of the puff above ground plays into its growth rate (via turbulent length scales), a representative height was set at 300 m to be consistent with the Oklaunion plume reported by Yarwood et al. The puff growth driver simulated size evolution over 6 hours.

Results from several test cases are tabulated in Table 4-1. The case labeled “Standard” employed the unmodified version of the puff growth algorithm from CAMx v5.40, where explicit shear was not included. The case labeled “Shear” included a nominal amount of horizontal and vertical shear. The case labeled “PBLx” was equivalent to “Standard” but had the depth of the nighttime residual layer increased from 100 m to 1000 m. The case labeled “q^2-L” was the same as “PBLx” but had the horizontal turbulent length scale reduced from 1000 m to 300 m and minimum turbulent energy reduced from 0.25 to 0.1 m^2/s^2. PiG dimensions given in black denote puff horizontal areas below 4 km grid scale, whereas dimensions given in blue would dump to a 4 km grid, and dimensions in red would dump to a 12 km grid (assuming circular puffs).

Table 4-1. Horizontal size evolution of a single test puff under idealized stable conditions for four different growth rate configurations (see text for details). Puff widths are given in terms of "full width at half maximum" (FWHM). Values in black represent puffs below 4 km grid scale; value in blue would cause puff dumping to a 4 km grid; values in red would cause puff dumping to a 12 km grid.

Hour Since Release	FWHM Puff Width (km)			
	Standard	Shear	PBLx	q^2-L
1	3.0	3.8	1.7	1.4
2	5.0	8.4	2.4	2.1
3	6.6	14.6	3.0	2.6
4	7.9	23.3	3.5	3.0
5	9.0	35.8	3.9	3.4
6	10.0	53.7	4.3	3.7

The "Shear" case is remarkably consistent with the first PiG run reported by Yarwood et al., and the "Standard" case is consistent with the final no-shear PiG run reported by Yarwood et al. This suggests that the idealized stable conditions set up in the external test driver were representative of the meteorological conditions on the night of October 10, 2006. The "Standard" puff remained three times wider than aircraft measurements in the 1-3 hour range. The addition of shear influences on puff growth were substantial, even with a modest amount of shear, leading to puffs that would last less than 1 hour before being dumped to a 4 km host grid, and just about 2 hours before being dumped to a 12 km grid (as reported by Yarwood et al.).

A variety of intermediate cases were run (not all shown) to test puff response to several parameters that control the growth rate. In one case, the depth of the nighttime residual layer was reset from 100 m to 1000 m ("PBLx"), consistent with CAMx versions prior to v5.40. This one change dramatically reduced puff growth rates, opposite of expectations. The reasoning is this: in the "Standard" case, the puff at 300 m was above the 100 m residual layer (meaning it was in the free atmosphere) and so the growth equations used the full 1000 m turbulent mixing length assigned to the stable free atmosphere, leading to enhanced growth rates. In contrast, the "PBLx" puff remained within the 1000 m residual layer, and so the free-atmosphere turbulent mixing length was scaled down according to plume height (resulting in an effective mixing length of 163 m), leading to reduced growth rates. Puff widths in the "PBLx" case were roughly half the values of the "Standard" case, and more in line with the flexi-nested run and aircraft measurements reported by Yarwood et al. In hindsight, the reduction of the residual layer from 1000 m to 100 m employed in CAMx v5.40 by Yarwood et al. inadvertently maintained large puff growth rates at night by placing most puffs into the "free atmosphere".

A final case called "q^2-L" was run in which the free-atmosphere values for the default mixing length and minimum turbulent energy were reduced. The reduction in energy was to quantify the sensitivity of puff growth to this parameter, whereas the reduction of mixing lengths from 1000 m to 300 m was to provide a smoother (i.e., less abrupt and arbitrary) transition in puff growth rates across the residual layer height. With this change to mixing length, puff behavior

within the residual layer would not be altered, but puff growth in the free atmosphere would be reduced to the value at the top of the residual layer. The resulting puff sizes were only marginally smaller than the "PBLx" case. Nevertheless, since puff sizes in the 1-3 hour range were in excellent agreement with aircraft measurements (1-2 km) for similar downwind ages, the changes in the "q^2-L" case were adopted for testing in CAMx.

4.3 Results

Two CAMx runs were performed to evaluate ozone impacts from the PiG modifications. These runs used inputs obtained from TCEQ for the Rider 8 May 31 – July 1, 2006 episode, including the original vertical diffusivity files (no modified Kv inputs were used in these tests). TCEQ developed point source inputs that flagged various large NOx emitters for the PiG treatment. The CAMx "Base" run was configured exactly like the TCEQ base run and used the original v5.40 source code. The "PiG Modification" run had the same configuration, but applied the revised v5.40 that reflects the PiG changes described above. The LVISPIG flag was not turned on, so all PiG mass was visually sequestered from the gridded output fields until that mass was dumped from puffs to the grid.

The vast majority of ozone difference arising from the modified PiG treatment occurred during the first half of each day between about midnight and noon. Both positive and negative ozone impacts occurred, usually between ±10 ppb, but positive differences tended to dominate in terms of magnitudes and spatial extent. Prior to sunrise, the slower growing puffs were retained by PiG much longer, reducing the frequency of puff dumping to the grid and reducing plume impacts on surface ozone (usually leading to higher ozone due to less destruction from NOx). Just after sunrise, as the boundary layer grew and fumigated overnight puffs toward the surface, a larger number of existing puffs were dumped to the grid (leading to higher and lower ozone depending on the chemical situation). During the second half of each day, between noon and midnight, little differences in gridded ozone fields generally occurred as the PiG treatments in both runs exhibited similar behavior. On a few dates, however, some residual yet coherent ozone plume differences of ~10 ppb or less propagated through the 4 km grid during the midday hours, likely the result of minimal daytime boundary layer mixing and/or exceptionally different PiG-dumped mass during the morning hours.

Figure 4-1 and Figure 4-2 display surface ozone differences over the 4 km domain at two times: June 26 at 3 AM, representing an hour with some of the most abundant and widespread differences throughout Texas, and June 13 at 8 AM, when the maximum surface ozone difference occurred. During the night of June 26, a large number of plumes were retained within PiG puffs, leading to surface ozone increases reaching 10 ppb across Texas in the absence of NOx titration. The smaller negative differences in Figure 4-1 are likely caused by some puffs in the PiG Modification run dumping later than in the Base run and in a slightly different location due to differences in transport trajectories between PiG puffs aloft and gridded mass at the surface.

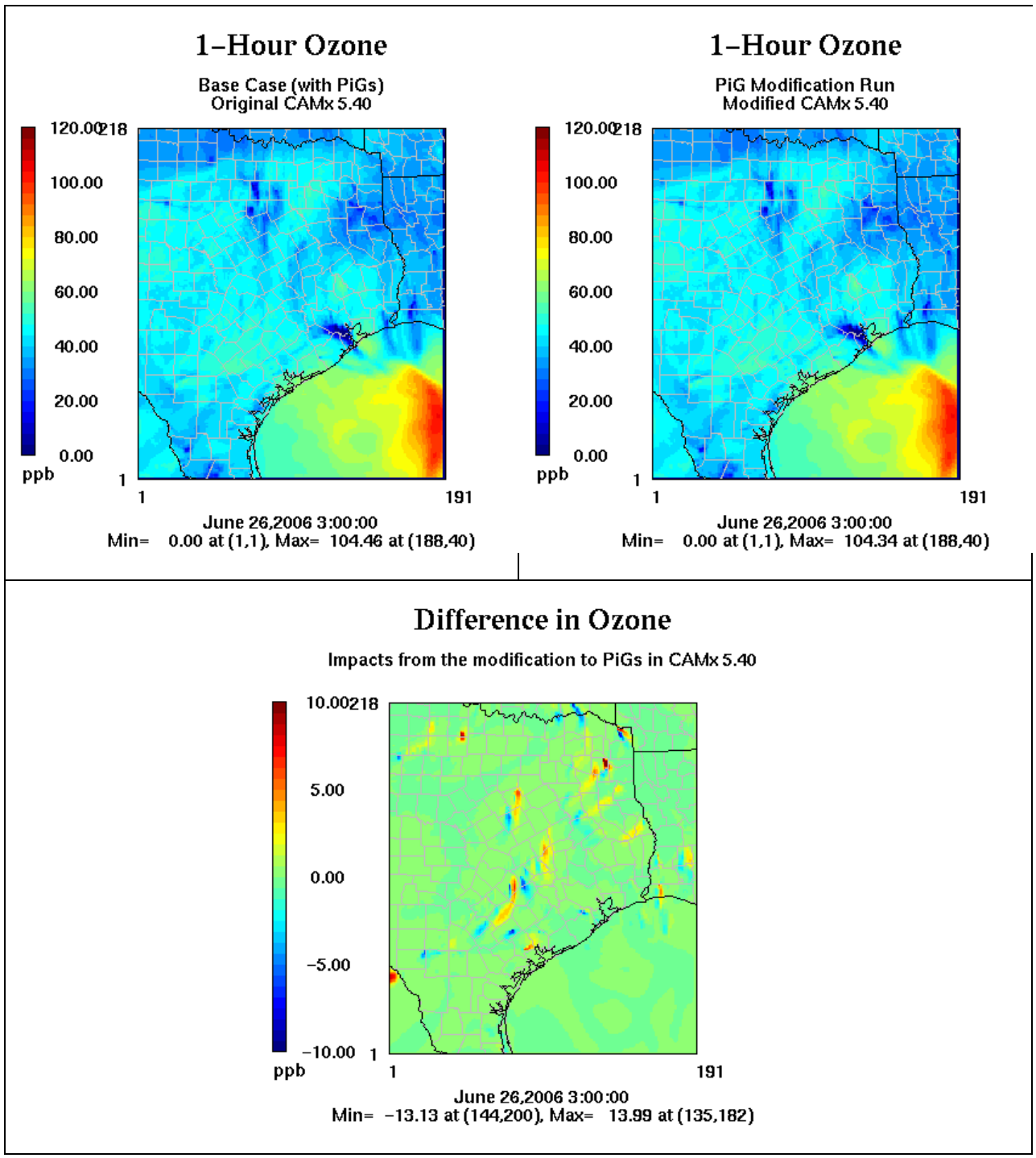

Figure 4-1. Simulated hourly ozone fields at 3 AM on June 26, 2006 for the Base run (top left), PiG Modification run (top right), and difference (bottom).

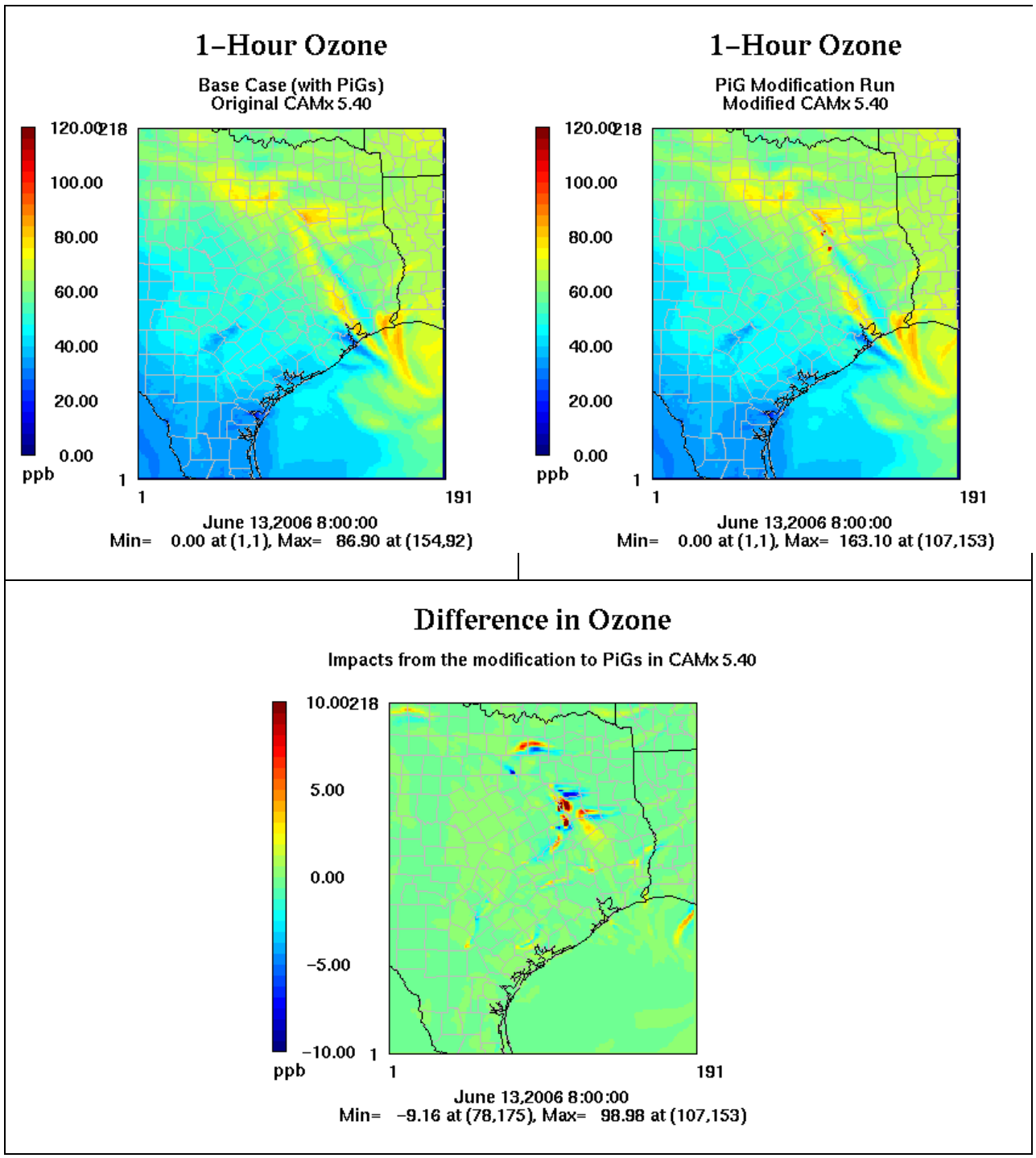

Figure 4-2. Simulated hourly ozone fields at 8 AM on June 13, 2006 for the Base run (top left), PiG Modification run (top right), and difference (bottom).

The maximum surface ozone difference of the episode reached nearly 100 ppb on June 13 in a single grid cell west of Palestine (over Lake Fairfield in Freestone County), raising local ozone from 64 ppb in the Base run to 163 ppb in the PiG Modification run (Figure 4-2). This was apparently caused by a sudden dumping of many converged puffs that had accumulated overnight, but these puffs were not capable of generating ozone themselves and dumping excess ozone to the grid. Therefore, the ozone enhancement was a chemical response on the grid to the dumping of accumulated semi-processed NOx emissions.

It would appear that the June 13 enhanced ozone event was the result of several factors in the model aligning to maximize the ozone impact from these PiG plumes. The peak ozone impact occurred along a convergence zone that formed overnight between Dallas and Houston, which can be seen in Figure 4-2 as a line of 70-80 ppb ozone, so this area was rich in preexisting ambient oxidants. It is also possible that persistently low boundary layer heights in the area of Lake Fairfield concentrated the ozone enhancement. The resulting ozone impacts slowly moved and diffused southward, decreasing to 60 ppb and 35 ppb differences at 9 and 10 AM, respectively, and to less than 10 ppb by 3 PM in Madison and Walker Counties just north of Houston.

The simulated peak ozone of 163 ppb on June 13 and the resulting surface ozone plume that subsequently moved slowly southward occurred in an unmonitored area, so the extent of this over prediction cannot be quantified. Given the severity of this event, and our current lack of understanding of the mechanism that caused it, we cannot recommend adopting these PiG changes in CAMx at this time. Additional in-depth investigation and potentially other improvements are necessary to eliminate chemically unrealistic PiG behavior.

4.3.1 Impacts at Rural Monitoring Sites

Most surface ozone differences caused by the PiG modification occurred in unmonitored areas of eastern Texas. For the vast majority of hours, predicted ozone concentrations at rural monitoring sites (Figure 4-3) were identical between the Base and PiG modification runs, with only occasional differences of several ppb in the time series. Figure 4-4 through Figure 4-6 show time series at Wamba, Clarksville, and Palestine monitoring sites, where the largest impacts from the PiG modification occurred among all rural sites in eastern Texas. The largest single-hour difference of 22 ppb occurred at Wamba, while maximum impacts at Clarksville and Palestine ranged between 4-8 ppb over just a few hours. As a result, there was no significant impact on statistical performance at these monitors. Time series and statistical performance analyses are not the optimum way to evaluate changes in point source plume behavior; comparisons to in-situ measurements (e.g., Yarwood et al, 2012) and emission sensitivity tests yield much more useful information.

4.3.2 Impacts on CAMx Runtime

Figure 4-7 compares the number of active puffs each hour in the Base and PiG Modification runs, averaged over the modeling period. The largest differences occurred during evening through late morning when the modified PiG puffs built up in all grids because they did not reach sizes for dumping. The relative increase in puff number correlated with grid resolution,

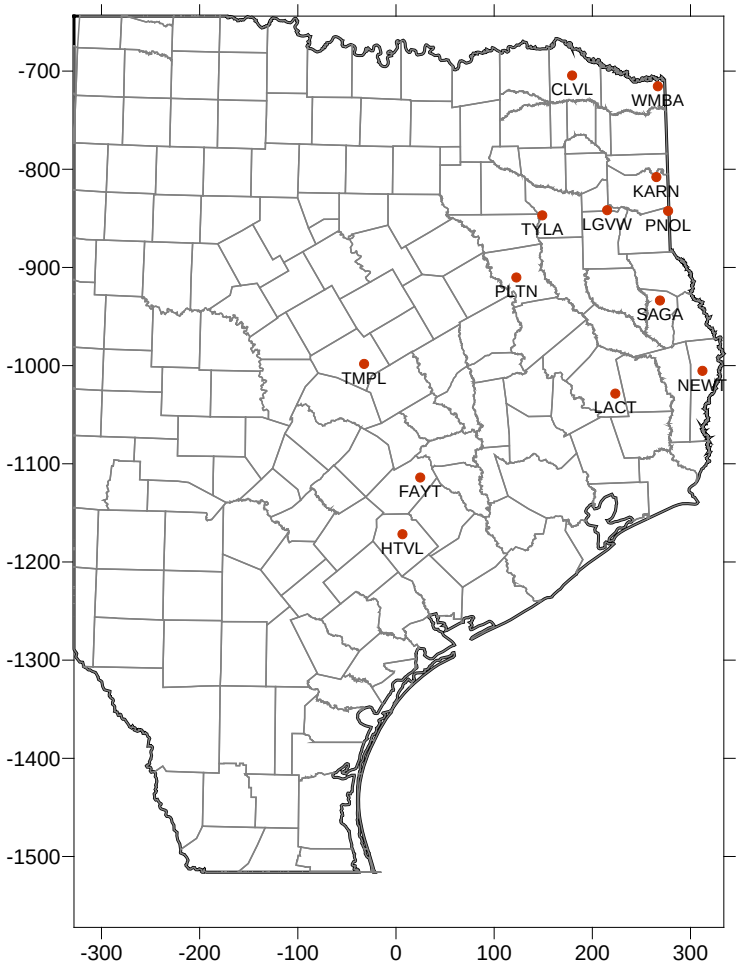

Figure 4-3. Rural ozone monitoring sites in eastern Texas evaluated for PiG plume impacts.

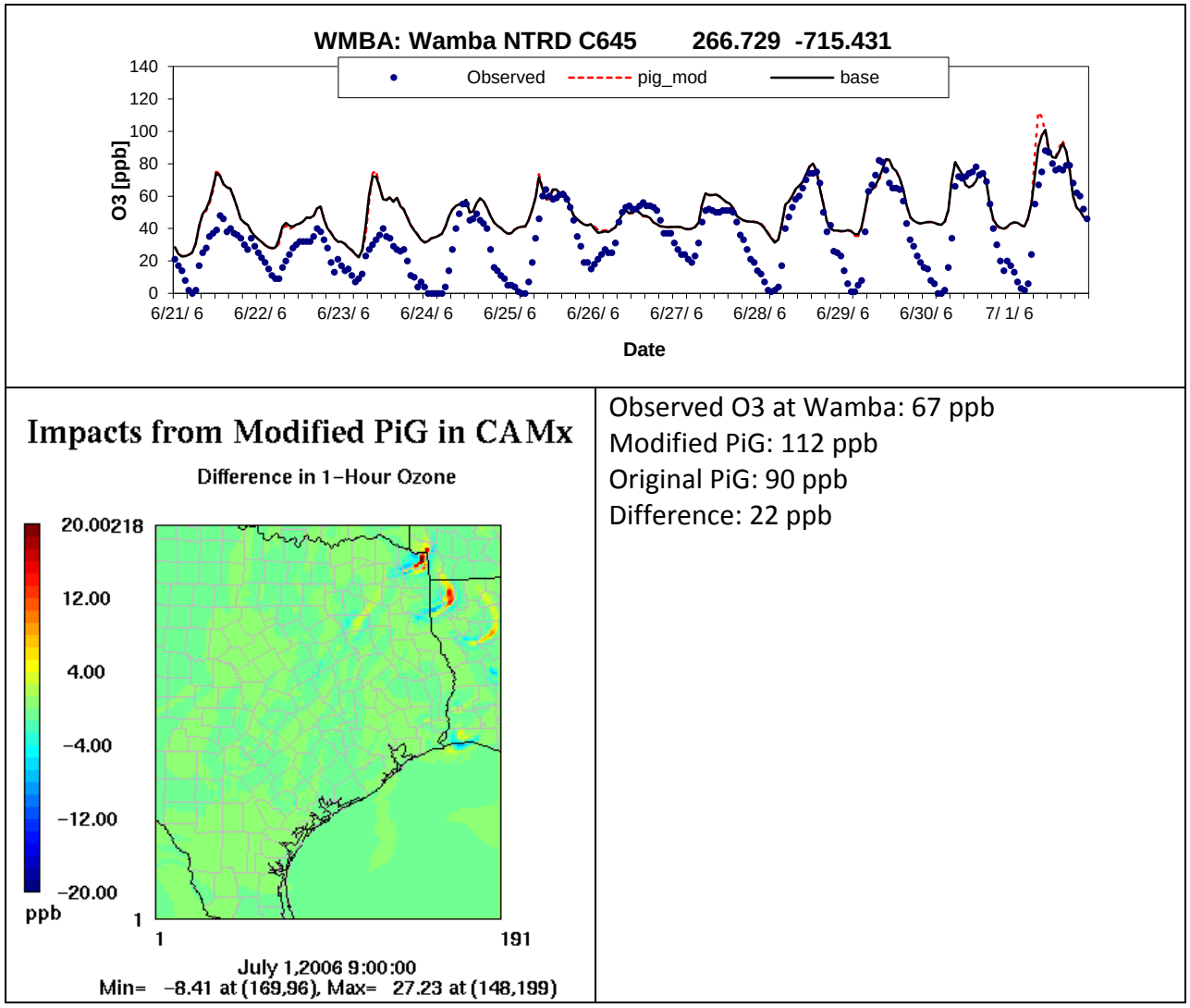

Figure 4-4. (Top) Time series of hourly observed and predicted ozone from the Base and PiG Modification runs at the Wamba monitoring site. (Bottom) Spatial distribution of hourly ozone differences between the Base and PiG Modification runs at the time of peak difference at the Wamba monitoring site.

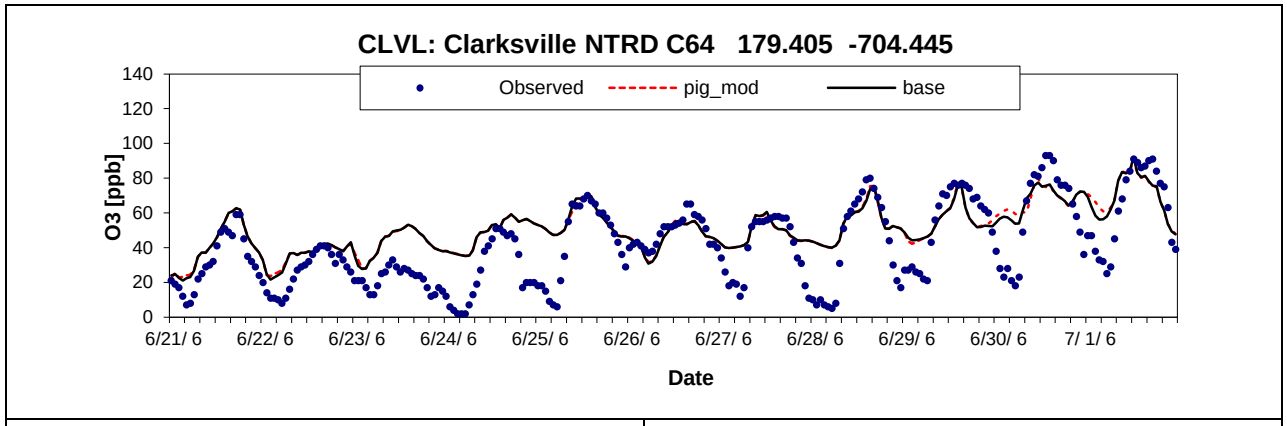

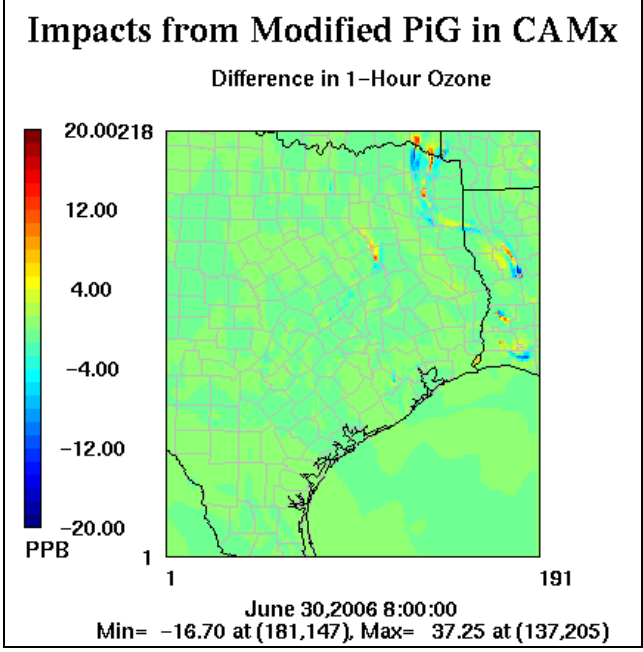

Observed O3: 67 ppb
Modified PiG: 60.2 ppb
Original PiG: 68.5. ppb
Difference: -8.2 ppb

Figure 4-5. (Top) Time series of hourly observed and predicted ozone from the Base and PiG Modification runs at the Clarksville monitoring site. (Bottom) Spatial distribution of hourly ozone differences between the Base and PiG Modification runs at the time of peak difference at the Clarksville monitoring site.

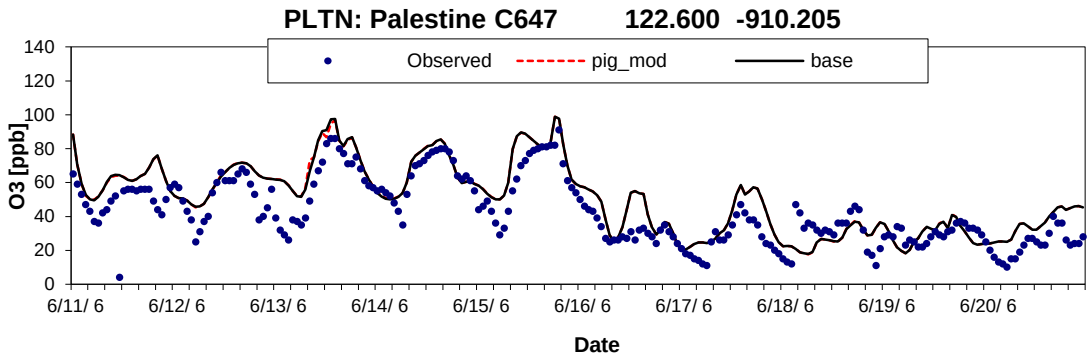

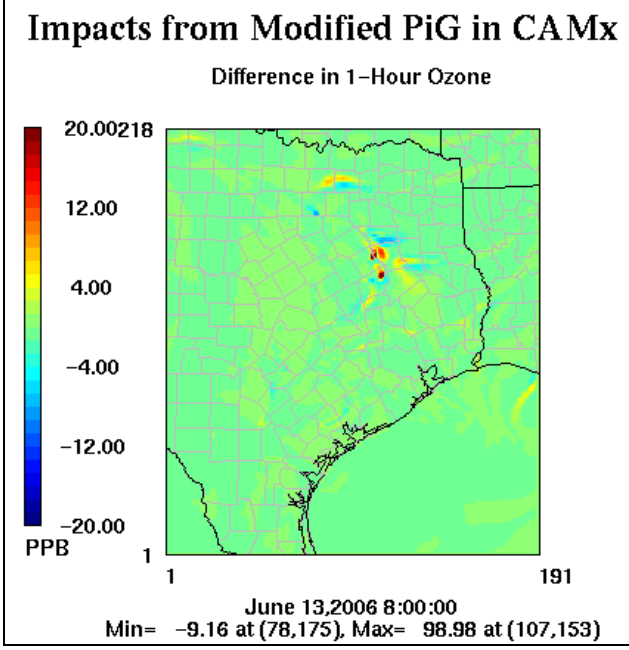

At Palestine
Observed O3: 49 ppb
Modified PiG: 73.3 ppb
Original PiG: 66.8 ppb
Difference: 6.5 ppb

Figure 4-6. (Top) Time series of hourly observed and predicted ozone from the Base and PiG Modification runs at the Palestine monitoring site. (Bottom) Spatial distribution of hourly ozone differences between the Base and PiG Modification runs at the time of peak difference at the Palestine monitoring site.

where the maximum increase in the PiG Modification run was 107%, 179%, and 208% in the 36, 12 and 4 km grids, respectively, between 7-9 AM. The rate of puff dumping during morning fumigation was also much steeper on the 4 km grid than the coarser grids. During daytime mixing, puff behavior was practically identical between the two runs, thus confirming that the impacts from the PiG modifications were reductions in puff growth mostly during stable nighttime conditions. Figure 4-8 shows day-specific hourly number of puffs in the Base and PiG Modification runs on the 4 km grid. Again, puff behavior day-to-day is consistent, with zero differences during the daytime and generally three times more puffs peaking around sunrise.

Running a significantly larger number of PiG puffs has implications for model run times. These CAMx tests were run using only OMP parallelization on a dual-quad core Intel Xeon (2.8 GHz) computer, where each CAMx simulation utilized all 8 cores. The Base run took an average of nearly 5 hours per day, while the PiG Modification run required about 30 minutes per day longer. Runtime performance impacts for MPI were not tested, and estimating them is complicated by several factors including MPI efficiency as a function number of CPUs employed, and the puff load for each MPI sub-domain. Therefore, MPI runtime performance impacts could not be extrapolated from these results.

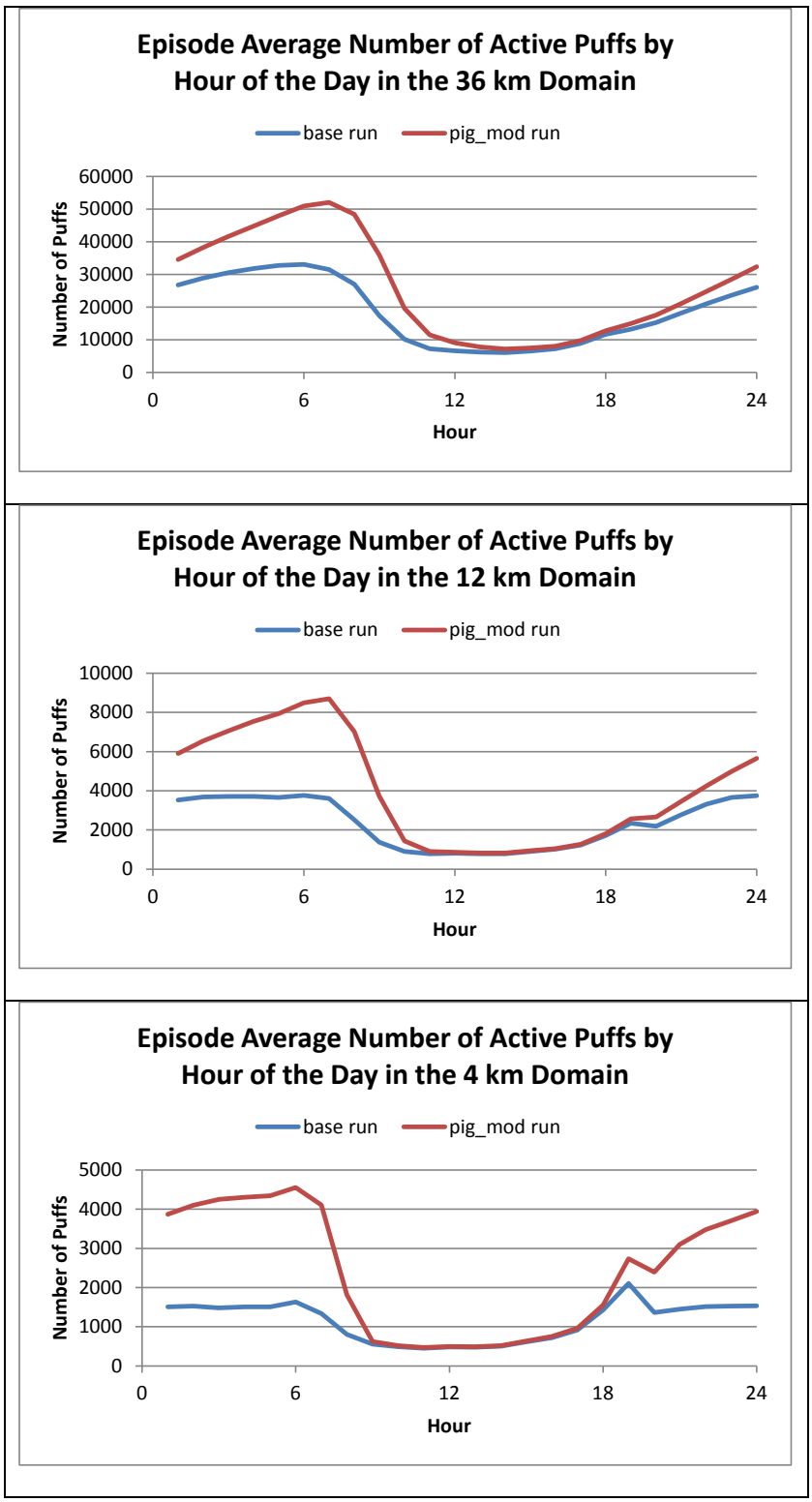

Figure 4-7. Average diurnal distribution of the number of CAMx PiG puffs in the 36 km (top), 12 km (middle) and 4 km (bottom) modeling grids over the June 2006 modeling period. Results from Base and PiG Modification runs are shown.

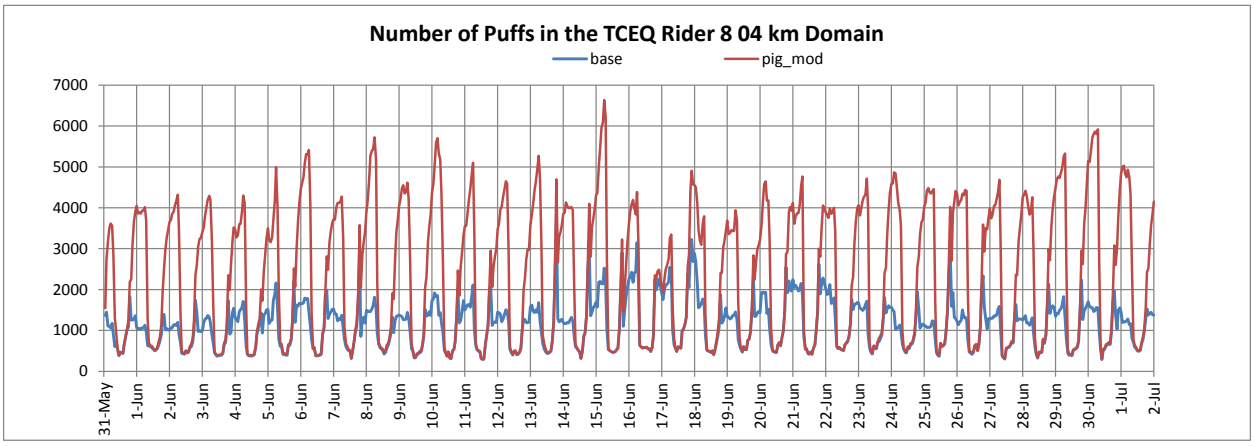

Figure 4-8. Number of CAMx PiG puffs each hour in the 4 km modeling grid over the June 2006 modeling period.

5.0 ENVIRONMENTAL FACTORS AFFECTING PHOTOLYSIS REACTIONS

The purpose of this task was to determine how strongly several environmental factors influence photolysis rates and to develop appropriate methods for representing these dependencies within CAMx. Sensitivity tests were performed using the TUV model. Photolysis rate dependencies on temperature and/or pressure were found to be small and can be accounted for by parametric adjustments within CAMx. Temperature and/or pressure adjustments were derived for photolysis of nitrogen dioxide (NO_2), ozone (O_3), formaldehyde (HCHO) and acetaldehyde (CH_3CHO). The influence of terrain elevation on photolysis rates is relatively small but has complex dependencies on other factors (e.g., zenith angle and molecular properties) that interfere with developing parametric adjustments. The next version of CAMx will explicitly account for terrain elevation in the photolysis rate input file. CAMx will continue to use pre-computed photolysis rates with adjustments (e.g., for cloud cover, aerosols, temperature, pressure) calculated within CAMx because this approach is far more efficient than the alternative approach of "in-line" computation of photolysis rates by a model such as TUV embedded within CAMx.

5.1 Technical Analyses

Photochemistry calculations within CAMx depend upon the rates of chemical reactions that are driven by sunlight (photolysis reactions). These photolysis rates are pre-computed using the TUV radiative transfer model (as described below). The pre-computed photolysis rate input file for CAMx accounts for variations in the following environmental factors:

- Properties of the molecule undergoing photolysis;
- Solar zenith angle;
- Height above ground;
- Light absorption by ozone in the stratosphere;
- Light scattering and/or absorption by aerosols (haze);
- Light reflection from the Earth's surface (UV albedo);

Other environmental factors that could influence photolysis rates are: (1) dependencies of molecular properties on temperature and/or pressure; and (2) terrain elevation above sea level.

Photolysis rates (J-values; s^{-1}) are determined by solar actinic flux (photons $cm^{-2}s^{-1}$), absorption cross section (σ; cm^2 $photon^{-1}$) and quantum yield (ϕ; dimensionless) all of which can vary with wavelength (λ). The wavelength-dependence of sunlight may be calculated using a radiative transfer model of the atmosphere, such as TUV (http://cprm.acd.ucar.edu/Models/TUV/), which describes how solar radiation propagating through the atmosphere is attenuated by absorption and scattering while at the same time enhanced by scattering and reflection from the ground. All molecules encounter the same solar actinic flux but have different J-values because σ and ϕ are characteristic properties of each molecule. Both σ and ϕ may vary with temperature and pressure although pressure-dependence of σ is not important for tropospheric conditions. Peer reviewed data for σ and ϕ are published by the IUPAC

Subcommittee for Gas Kinetic Data Evaluation (http://www.iupac-kinetic.ch.cam.ac.uk). IUPAC has published σ and ϕ temperature/pressure dependencies for photolysis of NO_2, O_3 and HCHO. Calvert et al. (2000) discuss temperature/pressure dependencies of ϕ for HCHO and CH_3CHO.

5.1.1 NO_2 Photolysis

Photolysis of NO_2 is important in the atmosphere because it is one of three reactions that lead to a photo-stationary state between NO_2, NO and O_3:

$$NO_2 + h\nu \rightarrow O + NO$$
$$O + O_2 \rightarrow O_3$$
$$O_3 + NO \rightarrow NO_2$$

The measured temperature dependencies of σ for NO_2 and ϕ for production of O-atoms from NO_2 are shown in Figure 5-1.

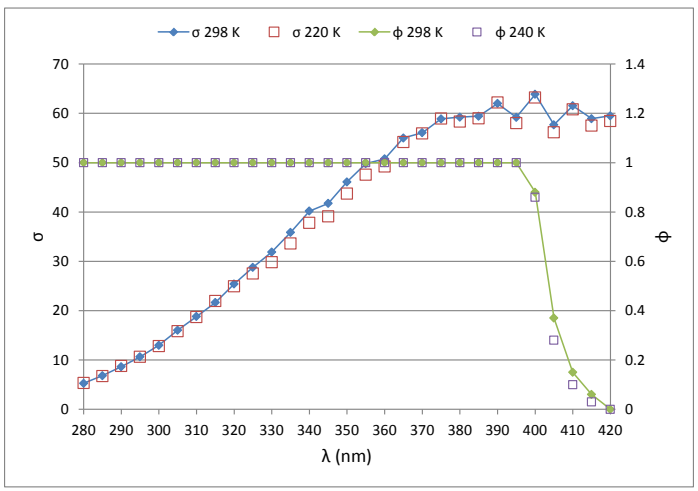

Figure 5-1. Absorption cross-section (σ; 10-20 cm^{-2}) for NO_2 and quantum yield (ϕ) for production of O-atom at UV wavelengths from 280-420nm.

5.1.2 O_3 Photolysis

Two reaction channels for O_3 photolysis are important in the troposphere producing oxygen atoms in their electronic ground state (O) or singlet-D electronic state ($O(^1D)$):

$$O_3 + h\nu \rightarrow O_2 + O$$
$$O_3 + h\nu \rightarrow O_2 + O(^1D)$$

Production of $O(^1D)$ is important because it is the main precursor to OH radical in the troposphere via reaction with water vapor:

$$O(^1D) + H_2O \rightarrow 2\ OH$$

The measured temperature dependencies of σ for O_3 and ϕ for production of $O(^1D)$ atoms from O_3 are shown in Figure 5-2.

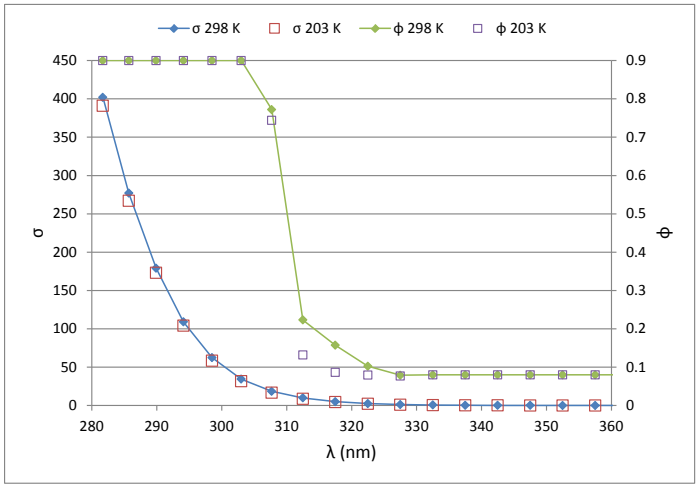

Figure 5-2. Absorption cross-section (σ; 10-20 cm^{-2}) for O_3 and quantum yield (ϕ) for production of $O(^1D)$-atom at UV wavelengths from 280-360nm.

5.1.3 HCHO Photolysis

Two reaction channels for formaldehyde photolysis occur in the troposphere forming either radicals (H and HCO) or molecular products (CO and H_2):

Channel 1: $HCHO + h\nu \rightarrow H + HCO$
Channel 2: $HCHO + h\nu \rightarrow CO + H_2$

Channel 2, producing radicals, is especially important because both H and HCO are quickly converted to hydroperoxy radical (HO_2) by reaction with O_2:

$H + O_2 \rightarrow HO_2$
$HCO + O_2 \rightarrow HO_2 + CO$

Figure 5-3 shows the measured temperature dependence of σ for HCHO.

Calvert et al. (2000) present an analysis of the temperature and pressure dependencies of the quantum yields for HCHO photolysis channels 1 and 2 (ϕ_1 and ϕ_2) and results from their methodology are shown in Figure 5-4. Both ϕ_1 and ϕ_2 are independent of temperature and pressure at wavelengths shorter than 330 nm. Beyond 330 nm, the sum of ϕ_1 and ϕ_2 falls below unity because energy removed by collisions from photo-excited HCHO molecules (collisional quenching) prevents some molecules from reacting. The efficiency of collisional quenching depends upon temperature and pressure. As shown in Figure 5-4, ϕ_2 increases at lower pressure because collisional quenching is less efficient. Lower temperature has a different effect than lower pressure on ϕ_2 because in addition to decreasing collisional

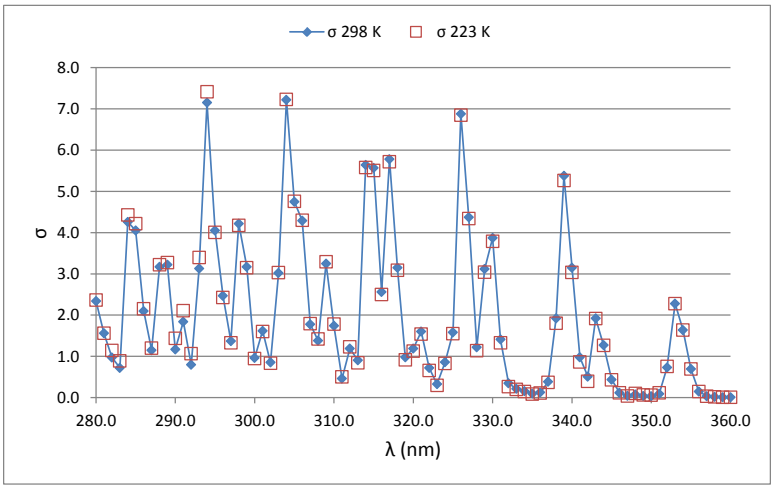

Figure 5-3. Absorption cross-section (σ; 10-20 cm^{-2}) for HCHO.

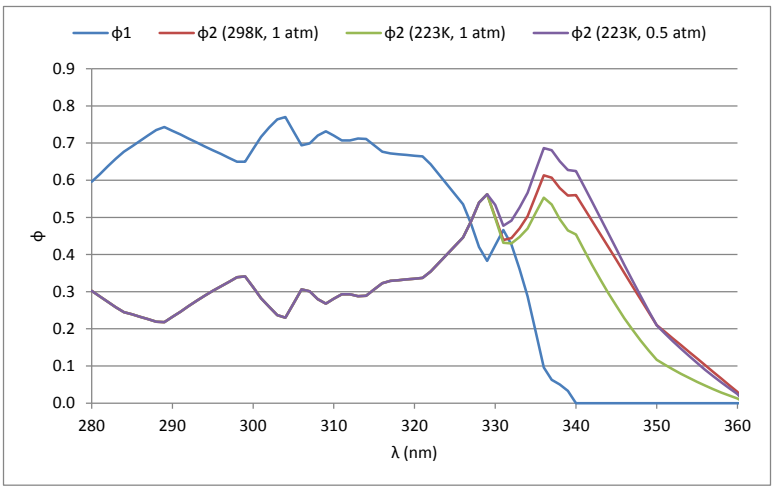

Figure 5-4. Temperature and pressure dependencies of the quantum yields for HCHO photolysis to HCO + H (ϕ_1) or CO + H_2 (ϕ_2). (ϕ_2 is independent of temperature and pressure.)

quenching (raising ϕ_2), the vibrational energy of HCHO molecules that assist photo-dissociation reactions is reduced (lowering ϕ_2). As shown in Figure 5-4, the net effect is that ϕ_2 decreases at lower temperature.

5.1.4 CH_3CHO Photolysis

Two reaction channels for acetaldehyde photolysis occur in the troposphere forming either radicals (CH_3 and HCO) or molecular products (CH_4 and CO) although the channel forming molecular products generally is neglected in atmospheric modeling. Reactions of CH_3 and HCO with O_2 produce HCHO, HO_2 and CO. No temperature dependence is reported for the σ for CH_3CHO (Figure 5-5). Calvert et al. (2000) present an analysis of the pressure dependence of ϕ

for CH_3CHO photolysis to CH_3 + HCO and results from their methodology are shown in Figure 5-6. ϕ rises with decreasing pressure because collisional quenching of photo-excited CH_3CHO molecules is less efficient at lower pressure.

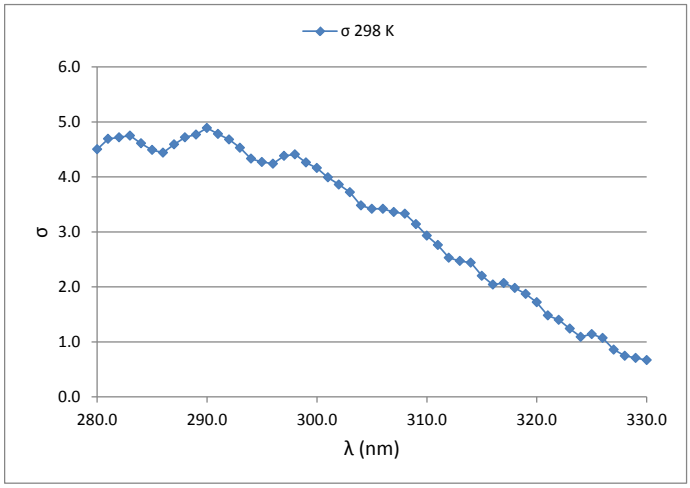

Figure 5-5. Absorption cross-section (σ; 10-20 cm^{-2}) for CH_3CHO.

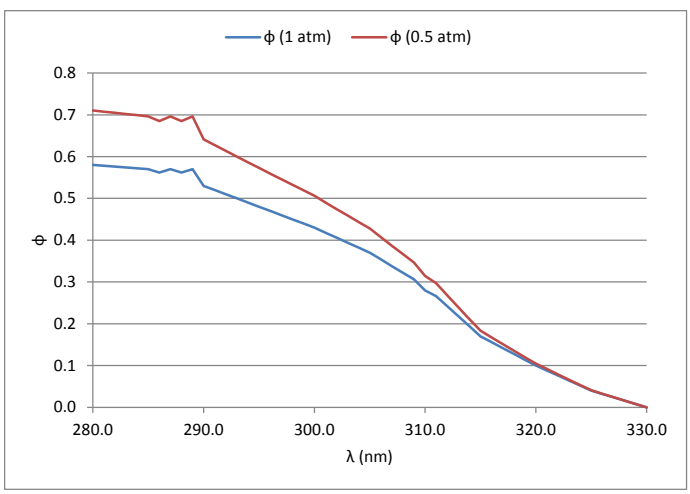

Figure 5-6. Pressure dependence of the quantum yield (ϕ) for CH_3CHO photolysis to CH_3 + HCO.

5.1.5 Using TUV to Calculate Photolysis Adjustment Factors

Sensitivity tests were performed using TUV to quantify changes in photolysis rates with temperature and pressure. Adjustment factors were calculated for ozone column of 300 Dobson units, UV albedo of 0.05 and 1 km above ground. In some cases, the variation of adjustment factors with solar zenith angle was sufficient to warrant taking into account (e.g. O_3

→ O(^{1}D)). The adjustment factors shown in Table 5-1 were incorporated into CAMx such that they are applied to the pre-computed photolysis rates as CAMx runs.

Table 5-1. Factors used in CAMx for adjusting pre-computed photolysis rates for temperature and pressure deviations from standard conditions of 298 K and 1 atmosphere.

Zenith Angle	Change with Temperature (per K)				Change with Pressure (per mb)	
	NO_2	O3 → O(^{1}D)	HCHO → H + HCO	HCHO → H_2 + CO	HCHO → H_2 + CO	CH_3CHO → CH_3 + HCO
0°	0.071%	0.265%	0.024%	0.033%	-0.017%	-0.021%
10°	0.072%	0.268%	0.024%	0.033%	-0.017%	-0.021%
20°	0.072%	0.275%	0.024%	0.033%	-0.017%	-0.021%
30°	0.072%	0.288%	0.025%	0.033%	-0.017%	-0.020%
40°	0.072%	0.308%	0.026%	0.033%	-0.018%	-0.020%
50°	0.073%	0.339%	0.026%	0.034%	-0.018%	-0.018%
60°	0.074%	0.384%	0.028%	0.034%	-0.019%	-0.017%
70°	0.076%	0.447%	0.030%	0.036%	-0.020%	-0.015%
78°	0.080%	0.485%	0.031%	0.036%	-0.021%	-0.012%
86°	0.081%	0.454%	0.032%	0.038%	-0.023%	-0.011%

5.2 Results

Two CAMx runs were performed to evaluate ozone impacts from the photolysis adjustments listed in Table 5-1. These runs used inputs obtained from TCEQ for the Rider 8 May 31 – July 1, 2006 episode; no modified Kv inputs were used in these tests and PiG was turned off. The CAMx "Base" run was configured exactly like the TCEQ base run and used the original v5.40 source code. The modified photolysis run had the same configuration, but applied the revised v5.40 that includes the new photolysis adjustments described above.

Overall the effect of these photolysis adjustments was to slightly change surface ozone concentrations during the daytime hours, but typically by only fractions of 1 ppb. Figure 5-7 displays the maximum and minimum ozone difference on the 4 km grid over the entire modeling episode; Figure 5-8 shows similar plots for the 36 km grid. The maximum positive 1-hour ozone impact over the entire modeling period was 0.7 ppb, with average daily maximum impacts between 0.3-0.5 ppb. The maximum negative change occurred off the coast of New York at -1.4 ppb. As suggested in both figures, the photolysis change resulted in widespread but small ozone changes that maximized during the midday hours. Ozone increases tended to be more frequent and widespread than ozone decreases. The positive effects of pressure are seen over the highest terrain in the 36 km grid. The separate effects of temperature vs. pressure adjustments were not evaluated.

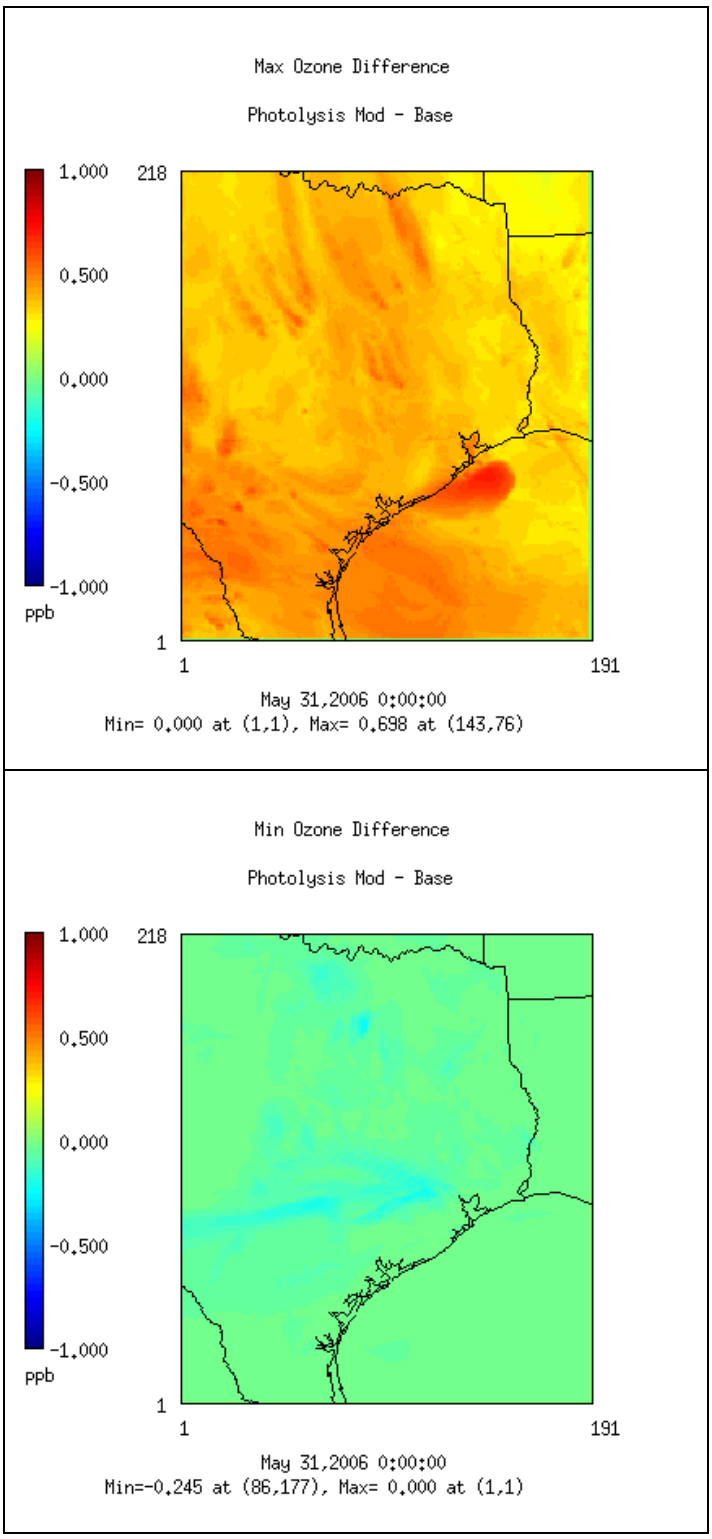

Figure 5-7. Maximum (top) and minimum (bottom) difference in simulated 1-hour surface ozone concentration (ppb) on the 4 km grid over the entire June 2006 modeling period resulting from the addition of temperature and pressure adjustments on photolysis rates for NO_2, O_3, HCHO, and CH_3CHO.

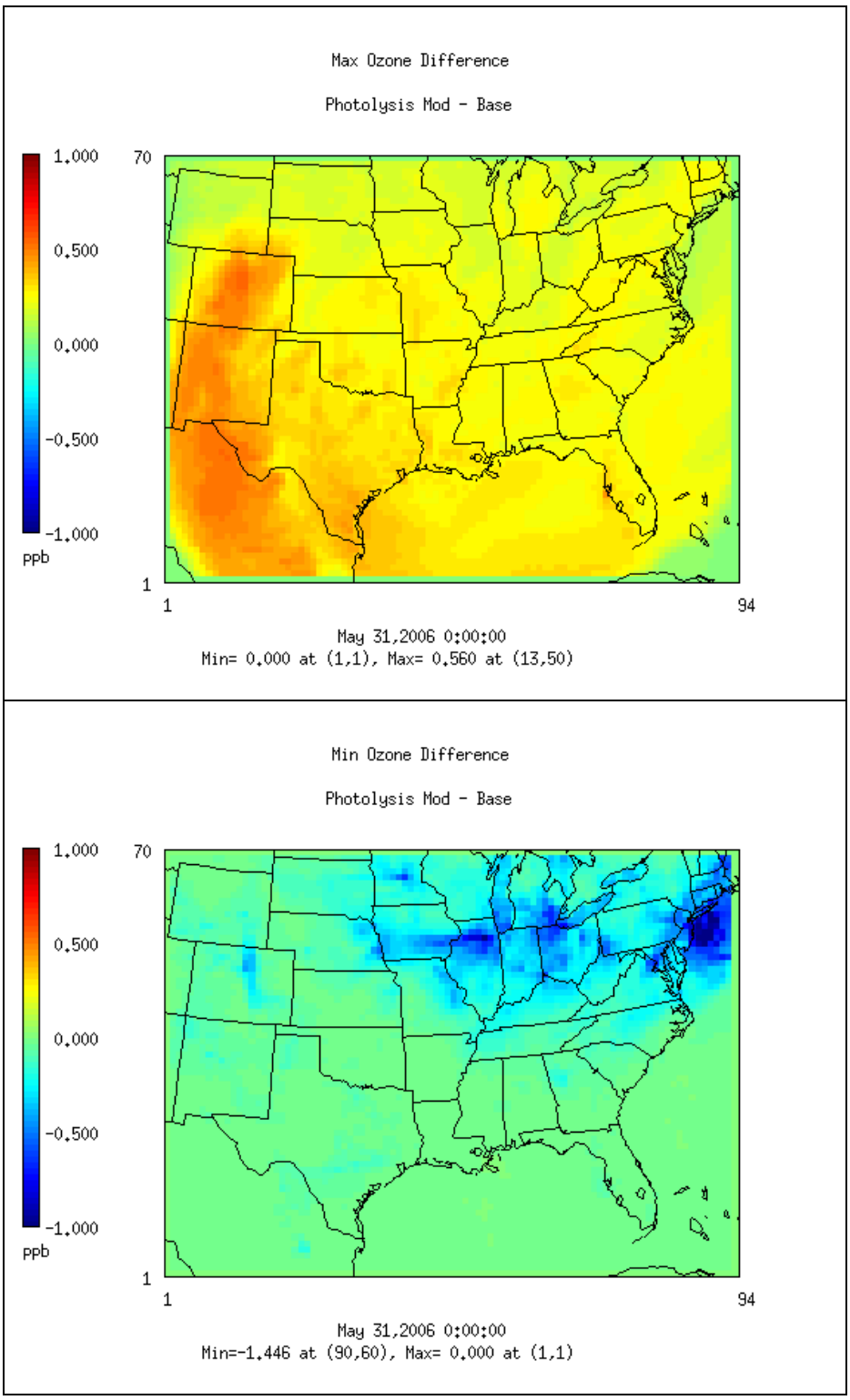

Figure 5-8. Maximum (top) and minimum (bottom) difference in simulated 1-hour surface ozone concentration (ppb) on the 36 km grid over the entire June 2006 modeling period resulting from the addition of temperature and pressure adjustments on photolysis rates for NO_2, O_3, HCHO, and CH_3CHO.

6.0 CONCLUSION AND RECOMMENDATIONS

6.1 WRFCAMx Efficiency Improvements

We have profiled WRFCAMx and note that the majority of runtime is spent in I/O processes (a total of 52% for this specific test case when writing across our network). We believe the test case documented herein is representative of a "large" application of WRFCAMx, but probably not the largest the TCEQ is likely to run. We were able to reduce runtime by 7% in the network I/O case, and 53% in the local I/O case, by taking advantage of the direct-access capabilities of the WRF netCDF output files.

It is important to note that WRFCAMx I/O speed may be significantly improved by reading and writing to a local disk drive. However, this must be balanced by the fact that WRF output data and CAMx input data would then need to be copied between a local drive and a remote system where these data are routinely archived. Overall time spent in transferring data before and after running WRFCAMx may eliminate any speed gains realized by running WRFCAMx with local I/O.

While OMP parallelization may be helpful to reduce runtime in calculating derived variable fields, the gains are small relative to the I/O issues described above. Therefore, we do not recommend adding this capability at this time.

ENVIRON has delivered to TCEQ a modified version of WRFCAMX (version 3.3) along with associated user documentation. Additionally, the modified version of WRFCAMx has been posted to the CAMx web site for public distribution.

6.2 Vertical Mixing Improvements

An updated KVPATCH program was developed to optionally apply one or more patches to the CAMx vertical diffusivity (Kv) files. The landuse patch was updated to revert the minimum Kv for forests back to 0.1 m^2/s (the urban minimum of 1 m^2/s was retained). A new OB70 patch replaced the previous KV100 patch to enhance low-level mixing in urban areas during nighttime hours. A new cloud patch raises the PBL and Kv profiles when cloud development collapses or suppresses daytime PBL mixing.

The new OB70 and previous KV100 patches yielded comparable ozone model performance against observations. Much of the nighttime differences outside of urban areas are attributed to the lower minimum Kv in grid cells containing forests. Both the landuse and OB70 patches target the nighttime hours, when the observed ozone in urban areas often drop below 40 ppb and thus are excluded from statistical performance measures. The KV100 patch consistently yielded the same or higher Kv's in layer 1, while the OB70 patch tended to produce higher Kv's in layers 2 and 3 after sunset. Both assisted in mixing some NOx out of layer 1 in the evenings, which helped slow down ozone titration. The new cloud patch raised PBL depths and Kv profiles when afternoon convection collapsed or suppressed vertical mixing. This helped to dilute daytime ozone, and was beneficial in areas where ozone was over predicted in the

presence of clouds. The performance impacts from the cloud patch are entirely dependent on the ability of the meteorological model to generate proper cloud distributions.

ENVIRON has delivered the modified version of KVPATCH and associated user documentation to the TCEQ. Additionally, the modified version of KVPATCH has been posted to the CAMx web site for public distribution.

6.3 Modifications to PiG Nighttime Growth Rates

We have tested modifications to the PiG growth algorithm that address turbulent length scales and minimum (stable) turbulent energy so that nighttime puff growth rates above the collapsed boundary layer are consistent with aircraft-measured plume widths at 2-3 hour transport times. An important component of this modification is the removal of explicit shear-induced puff growth; a new PiG flag was added to CAMx that allows the user to choose to ignore shear effects at all times or only during stable conditions. Properly simulating plume growth under such conditions is central to the proper characterization of plume chemistry and impacts on next-day ozone.

The PiG modifications led to a significant increase in the number of puffs overnight. This in turn resulted in the largest and most frequent impacts to surface ozone between midnight and sunrise (less PiG dumping resulting in less NOx titration and higher ozone), and between sunrise and noon (more NO_2 fumigating to the surface during boundary layer growth). Both positive and negative ozone impacts occurred (±10 ppb), but positive ozone differences were more common and tended to be larger in magnitude. Little surface ozone differences occurred between noon and sunset, as the PiG model behaved similarly between the Base and PiG Modification runs. Plume differences rarely coincided with monitoring sites in east Texas, with only occasional differences of up to a few ppb. As a result, there was no significant impact on statistical model performance at these monitors. Whereas afternoon peak ozone impacts from the PiG modifications were minimal in these tests with identical emissions, we expect that effects of NOx controls on next-day peak ozone would be considerably different, as demonstrated by Yarwood et al. (2012). Further tests with these PiG changes should include point source NOx reductions.

A single obviously faulty PiG-induced ozone impact reaching 100 ppb was simulated on the morning of June 13 in the PiG Modification test, but this occurred in an unmonitored area of Texas and so the extent of this over prediction cannot be quantified. Given the severity of this event, and our current lack of understanding of the mechanism that caused it, we cannot recommend adopting these PiG changes in CAMx at this time. We recommend additional in-depth investigation and potentially other improvements to the PiG algorithm to eliminate chemically unrealistic PiG behavior.

6.4 Photolysis Rate Adjustments

We have investigated the influence of several environmental factors on photolysis rates and have developed an efficient method to represent temperature and pressure dependencies within CAMx for four species: NO_2, O_3, HCHO, and CH_3CHO. Sensitivity tests were performed using the TUV model, from which parametric adjustments were developed and implemented in CAMx. Photolysis rate dependencies on temperature and/or pressure were found to be small, as were resulting surface ozone impacts. We conclude that the efficient parametric method implemented in CAMx to account for these factors is appropriate to the magnitude of the impacts. This approach is far more efficient than the alternative approach of "in-line" computation of photolysis rates by a model such as TUV embedded within CAMx.

ENVIRON has delivered the modified version of CAMx v5.40 to TCEQ. In addition, the next version of CAMx (v6.00) and its attendant TUV pre-processor will explicitly account for terrain elevation in the calculation of photolysis rates (this change was reserved for CAMx v6.00 because it substantially changes several input file formats).

7.0 REFERENCES

Calvert, J.G., R. Atkinson, J.A. Kerr, S. Madronich, G.K. Moortgat, T.J. Wallington, G. Yarwood. 2000. *The mechanisms of atmospheric oxidation of the alkenes*. Oxford University Press.

ENVIRON, 2011. "Dallas-Fort Worth Modeling Support: Improving the Representation of Vertical Mixing Processes in CAMx, Final Report." Prepared for the Texas Commission on Environmental Quality, Austin, TX. WO 582-11-10365-FY11-02.

O'Brien, J. 1970. "A Note on the Vertical Structure of the Eddy Exchange Coefficient in the Planetary Boundary Layer." *Journal of the Atmospheric Sciences*, 27, 1213-1215.

Yarwood, G., P. Karamchandani, C. Emery, S.-Y. Chen, S. Brown, D. Parrish. 2012. "NOx Reactions and Transport in Nighttime Plumes and Impact on Next-Day Ozone." Final report prepared for the Texas Air Quality Research Program, University of Texas, Austin, Tx. Prepared by ENVIRON International Corporation, Novato, CA; NOAA ESRL Chemical Sciences Division, Boulder, CO (January 31, 2012).